3D high-precision melt electro written polycaprolactone modified with yeast derived peptides for wound healing

Mahta Mirzaei, Gianina Dodi, Ioannis Gardikiotis, Sorin-Aurelian Pasca, Saeed Mirdamadi, Gilles Subra, Cécile Echalier, Chloé Puel, Rino Morent, Rouba Ghobeira, et al.

Graphical Abstract

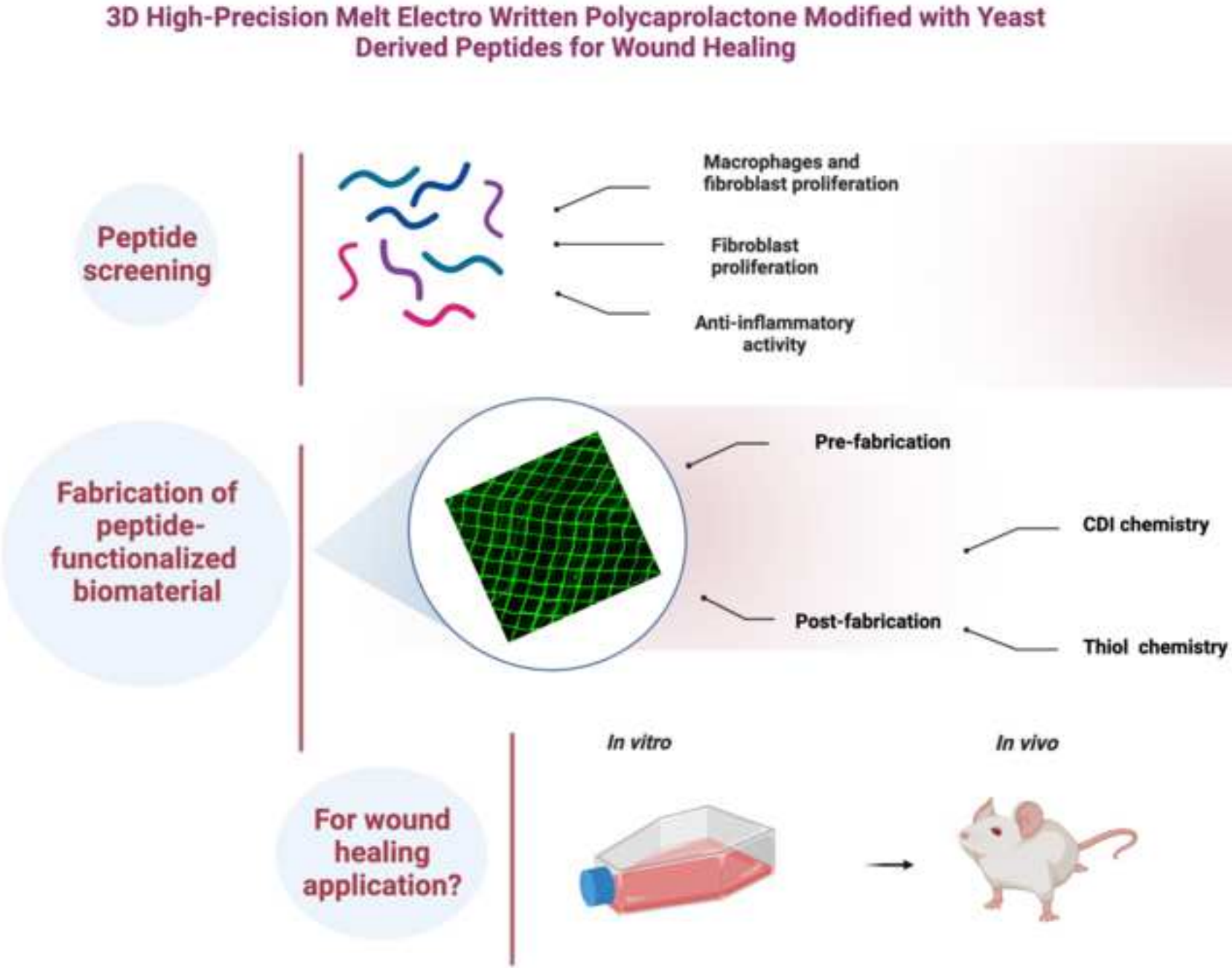

3D High-Precision Melt Electro Written Polycaprolactone Modified with Yeast Derived Peptides for Wound Healing

Mahta Mirzaei[a,b,c], *Gianina Dodi*[d], *Ioannis Gardikioti*[d], *Sorin-Aurelian Pasca*[e], *Saeed Mirdamadi*[f], *Gilles Subr*[g], *Cécile Echalier*[g], *Chloé Puel*[g], *Rino Morent*[h], *Rouba Ghobeira*[h], *Nazila Soleymanzadeh*[f], *Muriel Moser*[i*], *Stanislas Goriely*[i*], *Amin Shavandi*[a*]

a) Université libre de Bruxelles (ULB), École polytechnique de Bruxelles - BioMatter unit, Avenue F.D. Roosevelt, 50 - CP 165/61, 1050 Brussels, Belgium

b) Department of Environmental Technology, Food Technology and Molecular Biotechnology, Ghent University Global Campus, Incheon, South Korea

c) Department of Food Technology, Safety and Health, Faculty of Bioscience Engineering, Ghent University, Coupure Links 653, 9000, Ghent, Belgium

d) Advanced Research and Development Center for Experimental Medicine, Grigore T. Popa University of Medicine and Pharmacy of Iasi, Romania

e) Pathology Department, Faculty of Veterinary Medicine, Ion Ionescu de la Brad Iasi University of Life Sciences

f) Department of Biotechnology, Iranian Research Organization for Science and Technology (IROST), Tehran, Iran

g) IBMM, Univ Montpellier, CNRS, ENSCM, Montpellier, France.

h) Research Unit Plasma Technology (RUPT), Department of Applied Physics, Faculty of Architecture and Engineering, Ghent University, St-Pietersnieuwstraat 41 B4, 9000 Ghent, Belgium

i) ULB Center for Research in Immunology (U-CRI), Laboratory of Immunobiology, Université Libre de Bruxelles, Gosselies, Belgium

*Corresponding author 1:
Amin Shavandi
Postal address: Université Libre de Bruxelles, Ecole polytechnique de Bruxelles, Service BioControl, BioInfo and BioMatter (3BIO), Campus du Solbosch - CP 165/61, Avenue F.D. Roosevelt, 50, 1050 Bruxelles.
Email address : Amin.shavandi@ulb.be

*Corresponding author 2:
Stanislas Goriely
Postal address : Faculty of Sciences, Charleroi Campus - Gosselies (Biopark) - CP 300, Rue Prof. Jeener & Brachet, 12, 6041 Gosselies.
Email address : **:** Stanislas.Goriely@ulb.be

*Corresponding author 3:
Muriel Moser
Postal address : Faculty of Sciences, Charleroi Campus - Gosselies (Biopark) - CP 300, Rue Prof. Jeener & Brachet, 12, 6041 Gosselies.
Email address: muriel.moser@ulb.be

Abstract

In this study melt electro written (MEW) scaffolds of poly(ε-caprolactone) PCL are decorated with anti-inflammatory yeast-derived peptide for skin wound healing. Initially, 13 different yeast-derived peptides are screened and analysed using *in vitro* and *in vivo* assays, and then the MEW scaffolds are functionalized with the selected peptide of VLSTSFPPW (VW-9) with the highest activity in reducing pro-inflammatory cytokines and stimulating fibroblast proliferation, migration, and collagen production. Conjugation of the peptide to the MEW constructs are performed via carbodiimide (CDI) and thiol chemistry with and without plasma treatment and direct physical mixing of the peptide with polymer before printing. MEW plasma-treated scaffolds modified by CDI and thiol chemistry shows increased fibroblast and macrophage penetration and adhesion, as well as cell proliferation and superior anti-inflammatory action, compared to the other groups. Treating full-thickness excisional wounds in rat skin with free peptide and peptide modified MEW scaffold significantly enhancs the healing process as compared with controls ($p<0.05$). This study can provide a proof of concept for the application of yeast derived peptides in the functionalization of biomaterials for skin wound healing.

Keywords: yeast derived peptide, poly (ε-caprolactone), peptide-functionalized polymer, melt electro writing, wound healing

1. Introduction

Biocompatible and biodegradable polymer-based scaffolds can provide a three-dimensional environment, supporting cell adhesion and proliferation and delivering bioactive molecules and drugs to enhance tissue healing and regeneration[1]. Polymers such as polycaprolactone (PCL) are extensively employed in tissue engineering, and melt electrowriting (MEW) has been used to construct highly ordered polycaprolactone scaffolds with programmable design and geometry (PCL)[2].

However, the PCL scaffolds lack the bioactivity necessary for cell adhesion, proliferation, and desired response due to hydrophobicity and being biological inactive[3]. To improve cell compatibility or encourage desired cellular behavior such as cell proliferation and immunological response, it is preferred to modify PCL scaffolds to increase both hydrophilicity and introduce bioactive groups[4]. Plasma treatment is an effective way to increase the hydrophilicity of the polymer surface, and various bioactive compounds can be used to improve the functionality of PCL scaffolds[4]. For example, Hewitt, E., et al. (2019) reported the functionalization of melt-electrowritten PCL scaffolds with bioactive milk protein to increase the biological activity of skin regeneration scaffolds [5] and Nieuwoudt, M., et al., (2021) reported on the functionalization of electrospun PCL scaffolds with matrix-binding Osteocyte-derived extracellular vesicles to promote osteoblastic differentiation and mineralization[6].

Bioactive peptides have recently emerged as promising and cost-effective biomolecules for tissue healing and regeneration[7]. Antioxidant, anti-inflammatory, antimicrobial activities, as well as the ability to improve cell adhesion, and modulate immune responses are among the properties that make peptides desirable for functionalization of scaffolds[8, 9].

Techniques for scaffold functionalization include pre- or post-functionalization process. Pre-functionalization methods include physical or chemical interaction of peptide-polymer and fabrication of scaffold through different methods such as solvent-cast 3D printing[10], electrospinning[11] or melt-electrowriting[5]. For post fabrication, scaffolds are often modified by covalent linking or adsorption on the surface of biomolecules after the scaffold has been formed. Various approaches have been utilized to achieve peptide grafting, including EDC/NHS (1-ethyl-3-(3-dimethylaminopropyl)carbodiimide/N-hydroxysuccinimide), often known as the zero-length cross-linking reaction, which is the most frequently used process for functionalizing biomaterial through formation of amide bond between an amino group of polymer and carboxylic group of peptide. Thiol chemistry previously reported by De Luca, A. C , et al. (2012) was also employed for the functionalization of PCL following selective nucleophilic substitution of chlorine atom on the polymer surface by the thiol froming a cysteine residue[12].
We have previously deviated peptides VLSTSFPPK (VL-9) from *Kluyveromyces marxianus (PTCC5195)* and YGKPVAVPAR (YR-10) from the S*accharomyces cerevisiae* (PTCC5269) and developed their structural analogues, including VLSTSFPPW (VW-9), VLSTSFPPF(VF-9), VLSTSFCPK(VCK-9), VLSTSFYPK(VYK-9), VLSTSFHPH(VHK-9), STSFPPK(SK-7), YGKPVAVPAR(YR-10), YGKHVAVHAR(YHR-10), GKPVAVPA(GA-8),

GKHVAVHA(GHA-8), and PAR(PAR-3). We showed that these peptides have antioxidant, cytoprotective and angiotensin-converting enzyme (ACE)-inhibitory effects[13-15]. Given our findings and other studies [16-18], which showed that short peptides containing hydrophobic amino acids have powerful antioxidant, antibacterial, cell proliferation, and anti-inflammatory activities, it appears that these peptides could be used to improve the functional properties of biomaterials. These findings prompted us to first investigate the ability of these short yeast-derived peptides to influence microbial growth, cytokine production by macrophages, fibroblast proliferation, collagen synthesis, and cell migration, and then to use the selected peptide in combination with plasma treatment to improve the functional property of PCL scaffolds fabricated by melt-electrowriting.

2. Experimental Section/Methods

2.1. Peptides synthesis and purification

Thirteen different peptides indicated in Table 1 were synthesized chemically by SynthBio Engineering (Hefei, China) company using solid-phase approach with more than 95% purity. The IBMM (Institute of Biomolecules Max Mousseron, Montpellier, France) peptide team created a modified form of peptide VW-9 with an N-terminal Cys to enable the attachment to PCL by thiol chemistry using the procedure outlined in the supplemental file (S.1). Peptides containing biotin were also synthesized to facilitate characterization of peptides on the surface of scaffolds following labeling with Streptavidin and imaging using fluorescence microscopy. The peptides were synthesized by solid-phase peptide synthesis (SPPS), purified by reverse-phase preparative HPLC and analyzed by LC/MS. Detailed protocols are available in the supplementary information (S.1.6)

2.2. Poly-caprolactone (PCL) scaffold fabrication by melt-electrowriting (MEW)

Poly- caprolactone (Mw 80000 Da) powder was acquired from Polysciences, Inc (USA). A 3D-Bioscaffolder (Bioscaffolder 3.2, GeSiM GmbH, Großerkmannsdorf, Germany) was utilized for MEW, which combines pneumatic extrusion and high voltage induced fiber deposition. An aluminum cartridge with a temperature-controlled outer shell coupled to a conic aluminum nozzle with a 250 µm diameter orifice (Vieweg GmbH, Kranzberg, Germany) was used for printing. The nozzle-to-collector distance was 10 mm. The cartridge temperature was set at 95 °C, the plotting speed at 10 mm/s and the pressure set to 12 kPa. A glass plate provided by GeSiM used for collecting the MEW scaffolds. A square box-shaped scaffold (40 ×40 mm^2) was designed with 16 layers of parallel lines equally interspaced with subsequent layers positioned at a 90 ° angle to the previous layer. The height of the scaffold was set to 500 µm in the GesiM Robotics software.

2.3. Plasma treatment and surface characterization of the scaffolds

PCL scaffolds were subjected to an argon plasma treatment using a parallel-plate dielectric barrier discharge (DBD) operating at an Ar flow rate of 1 standard liter per minute (slm), a medium pressure of 5 kPa, a discharge power of 1.4 W and an exposure time of 15 s, according to the method described by Ghobeira et al. 2019 [19]. The surface chemical composition and

morphological properties of untreated and plasma-processed scaffolds were evaluated by X-ray photoelectron spectroscopy (XPS) and scanning electron microscopy (SEM) respectively. For the XPS measurements, a PHI 5000 VersaProbe II spectrometer equipped with a monochromatic Al Kα X-ray source (hν = 1486.6 eV) was used. Once the scaffolds were placed on the XPS platen and moved to the analyzing chamber, an exclusive X-ray beam induced secondary electron image camera (SXI) permitting accurate navigation over the scaffolds was employed to make sure that the analysis spots were precisely selected on the scaffold struts and not outside. Thereafter, these spots were excited with an X-ray beam (size: 100 µm) at a power of 25 W. Survey scans were acquired at a take-off angle of 45° with respect to the sample surface with a pass energy and step size of 187.85 eV and 0.8 eV respectively. The obtained spectra were analyzed using the Multipak (V 9.6) software to determine the surface elemental composition of the untreated and plasma-treated samples. The reported results are the mean values obtained from 4 independent analysis spots measured on 2 samples of each condition.
For the SEM measurements, a JSM-6010PLUS machine (JEOL, Japan) was used at an accelerating voltage of 7 kV. Before acquiring the images, the samples were coated with a thin gold layer making use of a JFC-130 autofine coater (JEOL, Japan).

2.4. Synthesis of peptide-functionalized scaffolds

Pre- and post-functionalization techniques were used to generate peptide-functionalized scaffolds. Physical pre-functionalization is the process of combining peptide with PCL powder and then printing scaffolds using MEWtechnique. For this purpose, several ratios of the peptide, 0.25, 1, and 2% (wt) were investigated.
For post-functionalization, scaffolds were initially printed using MEW, and then the peptide was grafted using EDC/NHS carbodiimide (CDI) chemistry and thiol chemistry, with and without plasma treatment.

2.4.1. CDI chemistry

PCL scaffolds were immersed in a 10% wt/v hexamethylenediamine (HMD) (Sigma, USA) in 2-propanol solution (pH=7) for 3h at 40 °C, with continuous stirring. The aminolyzed scaffolds were then rinsed three times with distilled water. 1-ethyl-3-(dimethylaminopropyl) carbodiimide (EDC) (Sigma, USA), N-hydroxysuccinimide (NHS) (Sigma, USA) and peptide were dissolved in 2-N-morpholino-ethanesufonic acid (MES) buffer (0.1 M) (pH:5.5) at equal molar ratios and stirred for 24 h at room temperature. The amount of peptide grafted to each scaffold (20 mm^2, 12.5 mg) was 0.5 mg (4% w/w) [20].

2.4.2. Thiol chemistry

PCL scaffolds were immersed in a 10% wt/v 2-chloroethylamine hydrochloride (CEA, Sigma, USA)/water (pH:9) solution for 3 h at 40°C with steady stirring. The chlorinated films were then washed with distilled water and dried overnight. Peptide and Tris (2-carboxyethyl) phosphine hydrochloride (TCEP) (TCI, Japan) were dissolved in MES buffer 0.1 M (pH:5.5) and added to each scaffold at a molar ratio of 1:5. At room temperature, it was stirred for 24 h. The scaffolds were then washed and dried three times with distilled water. The amount of peptide supplied was the same (4% w/w) as in the CDI chemical procedure [12].

2.5. Characterization of the scaffolds

The morphology and dimensions of PCL scaffolds were examined using SEM. Samples were fixed with glutaraldehyde 2.5% in cacodylate buffer for at least 1 h. Then directly metallized with 20 nm of platinum before scanning using a FEI ESEM Quanta 200 using high vacuum and a 30 kV tension. The dimeter of the fibers was quantified by Fiji software.Fourier transform infrared (FTIR) analysis was used to assess the sample functionalization, comparing the different methods, by using ATR platinum Diamond 1 BRUKER alpha II spectrophotometer with 24 scans in wavenumber range of 4,000–400 cm^{-1}. To visualize the presence and distribution of peptides on the scaffold surface the printed scaffolds containing biotinylated peptide and unmodified PCL scaffolds were fluorescently labeled with streptavidin-fluorescein isothiocyanate (FITC) (Sigma Aldrich, Germany) which specifically binds biotin. Samples were fixed in paraformaldehyde 4% for 15 min at RT, then washed in PBS and blocked for 30 min at RT in BSA 0.5%. Then, Streptavidin-FITC was used at 125 µg/mL and was incubated for 1 h at room temperature. After washing, samples were disposed in IBIDI µ-dish 35mm imaging chambers and were observed on an inverted wide-field fluorescence microscope (Zeiss Axio Observer Z1) using a 10x/0.3 Plan NeoFluar objective. Images were analyzed on Fiji by segmenting the samples from the background using an intensity threshold and analyzing the mean intensity [10].

Elemental analysis was also performed by Elemental Analyzer (EuroVector, Italy) to measure the amount of Nitrogen in different scaffolds. To study the stability of the peptide under printing conditions (95 °C, 6h) a precise mass of peptide VW-9 was put in the oven at 95 °C. After 6 h, the peptide was analyzed by UPLC/MS and its spectra was compared with the control sample (before oven treatment). The samples were analyzed with an ACQUITY UPLC™ (Waters corp., USA) system with a ACQUITY UPLC Peptide HSS T3 column (100 A°, 1.8 µm, 2.1 mm× 50 mm, 1K-15K, 1/pK) equipped with a Zspray triple quadrupole mass spectrometer. The mobile phase included water with 0.1 % formic acid (A) and acetonitrile with 0.1 % formic acid (B). A gradient of 0-100% B over 4.5 min, a flow rate of 0.8 $mLmin^{-1}$, an injection volume of 5 µL, and detection wavelength of 214 nm were used. The data were obtained in a scan mode ranging from 100-1100 m/z in a 0.2 s intervals [21].

For quantification of peptide release from samples obtained by pre-functionalization method, scaffold A7 (40*40 mm^2, containing 1% (wt) peptide) was immersed in 10 mL of PBS at 37°C, and 200 mL of supernatant was sampled out at different times for examination of peptide release by UPLC/MS method as described for peptide stability test. A ACQUITY H class (Waters corp., USA) system plus UPLC equipped with a Zspray single quadrupole mass spectrometer was used for this purpose. A standard curve with concentrations of peptide ranging from 0.001 to 0.050 mg/mL was established to demonstrate the linear relationship between MS signal and concentration.

2.6. Cell culture and cell viability assay

U937, a pro-monocytic human myeloid leukaemia cell line (ATCC, CRL-1593.2) and fibroblasts (ATCC, CCL-186), were obtained from American Type Culture Collection. The cells were cultured in RPMI 1640 and DMEM medium respectively, supplemented with 2 mM L-Glutamine, 10% fetal bovine serum (FBS), and 100 unit/mL penicillin/streptomycin

(Lonza), according to ATCC guidelines. The U937 (passage number 12-16) and fibroblast cells (passage number 16-20) density were maintained at 400,000 and 100,000 viable cells/mL, respectively. Cells were incubated at 37 °C in a humidified atmosphere (5% CO_2). Cells were harvested once the cell confluency reached approximately 80-90%. U937 cells were differentiated to macrophage-like cells after being treated with PMA (300 nM) for 24 h followed by resting for another 24 h. We performed a real-time Glo MT assay (Promega, USA) to assess the viability of cells following treatment of cells with different concentrations (0, 0.25, 0.5, 1mM) of peptides. At zero, 24 h, 30 h and 48 h time intervals, luminescence intensity (RLU) was monitored continuously using a microplate-reading luminometer (Promega, GloMaX) [22].

For cell culturing on the scaffolds, the U937 and fibroblast cell lines were detached from the flasks, centrifuged, and resuspended in culture media. Cell survival was determined by MTS test. In a 24-well plate, U937 cells and fibroblasts (5×10^4) were planted on scaffolds at the bottom of each well. Scaffolds were trimmed to a size of 10×10×1 mm to fit inside a 24-well plate's transwells. The scaffolds were disinfected by immersing them in 70% ethanol for 24 h, then washing them in PBS and exposing them to UV radiation for 30 minutes. Cells were seeded at a density of 50,000 (for cell viability experiments) and 200,000 (for ELISA and imaging assays) cells/mL onto each scaffold initially. In a volume of 20 µL, cells were seeded directly onto each scaffold, incubated for 30 minutes, and then 1 mL of medium was added to each well [5].

2.7. Fluorescence cell characterization on scaffolds

Fluorescent staining was used to visualize placement of macrophages and fibroblasts on the selected scaffold (A3) and control scaffolds A0 (native PCL) and A2 (plasma treated PCL).

U937 and fibroblast monolayers were seeded on scaffolds (10*10 mm) in a 24 well plate at a total density of 200,000 cells/well and allowed to develop for 48 h. The scaffolds were placed in a new 24-well plate and rinsed twice with PBS before being fixed with a 4% paraformaldehyde (PFA) solution for 15 minutes at room temperature then washed in PBS and permeabilized by Triton X-100 0.2% for 5 min at RT. After blocking in 0.5 % BSA for 30 min at RT, Alexa Flour 488 Phalloidin (Abcam, ab176753, used at 1:1000 of stock solution) in blocking solution was added for 90 min at RT. Samples were washed, counterstained with DAPI (Thermofischer, USA) at 0.1 µg/mL for 3 minutes and then scanned using wide-field fluorescence microscope (Zeiss Axio Observer Z1) with a 10x/0.3 Plan NeoFluar or a 20x/0.5 Plan NeoFluar objective [23].

2.8. SEM cell characterization on the scaffolds

The cell fluorescence staining was complemented with SEM imaging of cells on the scaffolds to obtain a detailed visualization of cell morphology. SEM micrographs of the scaffold surface seeded by cells were taken after 48 h of cell seeding. Preparation of scaffolds as follow: Samples were fixed in glutaraldehyde 2.5% in cacodylate buffer for at least 1 h. Samples were post-fixed in osmium 2% in cacodylate buffer, then washed and dehydrated in increasing concentrations of methanol (30%-50%-70%-95%-100% for 15 minutes each). Pure methanol was replaced by HMDS (hexamethyldisilazane) 100 % which was left for drying under

chemical hood for a few days. Once samples were dried, they have been metallized with 20 nm of platinum before scanning using a FEI ESEM Quanta 200 using high vacuum and a 30kV tension [19].

2.9. Anti-inflammatory activity

In this study, we employed U937 as an *in vitro* model for investigating inflammatory markers and macrophage activation by LPS and IFN-γ.Immunomodulatory activity of the peptides was assessed by seeding U937 at 400,000 cells in 2 mL per well in 24-well plates. Following PMA treatment (300 nM, 24 h) and resting for 24 h, U937 cells were pretreated with peptides for 22 h, followed by stimulation of cells with Lipopolysaccharide (LPS) (*E. coli* O55: B5, Sigma) (500 ng/mL) for 6 h or 19 h to evaluate the production of TNF-α and IL-6 by flow cytometry and Enzyme-linked Immunosorbent Assay (ELISA) methods, respectively. Cells were pretreated with peptides and treated by recombinant Interferon-gamma (IFN-γ) (20 ng/mL) for 24 h for evaluation of CD64 surface expression. The anti-inflammatory mechanism of most active peptides was investigated by evaluating its influence on regulation of the NF-κB and p38 MAPk pathways and expression of anti and pro-inflammatory cytokines genes using the methods described in supplementary file (S2).

To assess the anti-inflammatory activity of peptide-functionalized scaffolds, PMA-treated U937 cells were cultured on scaffolds (10×10×1 mm), placed in the bottom of each well at concentration of 200,000 cells in 1mL per well. Cell stimulation was performed as explained for peptide samples and the levels of TNF-α and IL-6 were evaluated by ELISA method [24].

2.9.1. Flow cytometry analysis

After stimulation, U937 cells were subjected to staining using anti TNF-α antibody (Clone Mab11, conjugated with Alexa fluor 700) and anti-CD64 monoclonal antibody (clone 10.1, conjugated with FITC) (Invitrogen). To determine the amount of TNF-α, cells were treated with Brefeldin A (Invitrogen, USA) at a final concentration of 3 µg/mL for 6 h before staining. Live/Dead fixable Near-IR dead cell stain kit (Thermofisher, USA) was utilized in all experiments to assess cell viability. Before intracellular staining, fixation, and permeabilization/wash buffer (Invitrogen, USA) were used. After 30 min staining at 4°C, cells were washed with PBS and suspended in PBS for analysis by FACS Calibur Flow cytometer (Becton Dickinson). Fluorescence intensity analysis was performed using a FlowJo (Version 10.7.1, Treestar Software, USA). After separating the possible noises, by selecting the main population in the side scatter area vs forward scatter area [FSC-A], single cells were selected using forward scatter height vs FSC-A plot for further analysis.

2.9.2. Enzyme-linked immunosorbent assay (ELISA)

Supernatants were collected to determine TNF-α and IL-6 with specific ELISA kits according to manufacturer`s instruction (DuoSet ELISA Development System, Biotechne). Optical density was read immediately using a microplate reader at 450 nm and cytokine concentrations were evaluated using a standard curve.

2.10. Wound healing scratch assay

The peptides were tested for *in vitro* wound healing activity using wound scratch assay. Fibroblast cells were seeded (100,000 cells/well) in 2 mL in 48-well plates and allowed to grow for 24 h. When the cells reached 100% confluence, the monolayer of cells was scratched with a yellow pipette tip to create a scratch and washed twice with PBS to remove floating cells. Each well was filled with 1 mL DMEM (with 2% FBS) containing peptides at a final concentration of 0.5 mM. Throughout the 24 h period, images of wounded cell monolayer were taken every six hours using a Zeiss AxioObserver Z1 (inverted wide-field microscope) with a 10x/0.3 EC Plan Neofluar Dry Ph1 objective. Fiji software was used for image analysis [25]. The migrated cells were imaged, and the covered areas were measured using the WimScratch software program (Wimasis, Munich, Germany).

2.11. Collagen production by fibroblasts

In 24-well plates, fibroblasts were seeded at a density of 50,000 cells per 2 mL. 24 h later, the cells were treated with various concentrations of the peptide for 24 h. The collagen concentration in 20 µL of two-times diluted supernatant samples was measured using a collagen assay kit (MAK322, Sigma- Aldrich, USA) and a fluorescent microplate reader (BioTeck, USA) at $\lambda ex = 375/\lambda em = 465$ nm.

2.12. Antimicrobial activity

Escherichia coli (ATCC 25922) and *Staphylococcus aureus* (ATCC 25923) were acquired from the Persian Type Culture Collection (PTCC). Strains were cultivated on nutrient agar (Lab-Lemco powder 1.0 g/L, yeast extract 2.0 g/L, peptone 5.0 g/L, NaCl 5 g/L, agar15 g/L) and antimicrobial activity testing were conducted using Mueller Hinton broth (Scharlu, Spain). The antimicrobial activity of the synthesized peptides was determined using the CLSI-recommended microdilution method (M7-M100, 2018) [26]. The bacterial inoculum was prepared by direct colony suspension method in normal saline (OD_{600nm} = 0.1- 0.12). The suspension was then prepared in Mueller Hinton broth at a concentration of 10,000000 CFU/mL. In 96-well round-bottom microplates, 50 µL of a 1000,000 CFU/mL suspension of bacterial was added to peptide solution at a gradient concentration range of 0.02 -10 mM. The microplates were incubated at 37 °C for 16-20 h. The minimal inhibitory concentration (MIC) was defined as the lowest concentration of peptide at which there was no bacterial growth. To estimate the minimal bactericidal concentration (MBC), we used the spread plate method to culture the whole content of the wells with no growth on a nutrient agar medium.

2.13. Wound healing assay

Adult male Wistar rats (300-450 g, 14 or 5 months of age) were housed in temperature- and humidity-controlled individually ventilated cages (12:12-h light-dark cycle) with free access to water and a standard pellet diet. The animal experiments were performed according to international guidelines and were approved by the Ethical Committee of the Grigore T. Popa University of Medicine and Pharmacy of Iasi, Romania. The rats were divided into four groups (5/group) as follows:

- group 0 (blood donors, sacrificed to prepare platelet-rich plasma -PRP- solution);
- the PRP group (positive control group, C1+);
- the peptide group (test group containing VW-9, 0.5 mM) ; and
- tested scaffold group (T).

Rats in group 0 were anesthetized by inhalation with isoflurane gas mixed with normal air (5% for induction and 2% maintenance), and 10-14 mL of blood was drawn via the central abdominal artery and introduced into clear tubes. The rats were euthanized after blood harvest through exsanguination and during 5% isoflurane hyperdose. Blood cell elements were separated using a laboratory centrifuge (Universal 32R, Hettich, Germany) at 3500 rpm (1317 RCF) for 5 minutes at 20°C, resulting in two basic components: red blood cells at the bottom and platelet plasma on top, yielding 3-4.5 mL. The platelet-rich layer was separated by further centrifugation, in different tubes, at 6300 rpm for 20 min, and the PRP solution (1 mL) was isolated from the supernatant and stored at 4°C until use. The PRP isolation process was freshly prepared for each experimental day during the entire study.

The back of the rats from the three remaining groups was shaved, and the skin was cleaned with chlorhexidine di-gluconate (20%, 10.65 mg) and benzalkonium chloride (50%, 9.85 mg) solution. In the groups C1+ and peptide, two circular full-thickness cutaneous wounds with a diameter of 1.5 cm were marked and were then carefully excised by using sterile sharp scissors. The wounds were made on the dorsal surface with one on each side and left undressed to the open environment. The right for the PRP (C1+) or VW-9 treatment and on the left for negative control (sterile pure water). The day of wound creation was defined as day 0 of the study. 50 µL solution of PRP or VW-9 were applied using a pipette to cover the wounded area twice per day up to day 7.

Three lesions of about 1.5 cm diameter were performed using the same procedure as above, equidistant 1 cm from each other to the back-midline of each animal for the tested scaffold group. Then, in each rat, the two wounds were treated with tested scaffold (T) and Sorbalgon® dressing (C+), both folded to cover the entire wound area, followed by two-layered retention cotton gauze. The third wound lesion was covered with cotton gauze and defined as the negative control. Wound dressings were changed after wound cleaning with saline solution, on day 4, 8, and 12 post-surgery and completely removed on day 16. For the animals' pain management, an intra-peritoneal injection of 40 mg/kg tramadol was used on the day of surgery (day 0). Photographs of the wounds were taken using a digital camera (Sony, model no. DSC-W570 with 16.1 megapixels) at days 0, 3, 5 and 7 for the first part of the study, and at each dressing change during the healing process.

The wound sizes were measured on the 3rd and 7th day for the PRP/peptide group and at 4th, 8th, 12th and 16th day for the scaffold group using a paper ruler. The wound-healing ratio (HR) was calculated by the equation as follows:

$$HR(\%) = \frac{S_0 - S_n}{S_0} \times 100 \,,$$

where S_0 and S_n are the wound areas at day 0 and the predetermined experimental day, respectively.

On day 3, 4, 7, 8, 12 and 16 respectively, the animals were euthanized by anesthesia hyperdose and the full thickness wound tissue with a minimum of 0.5 cm normal tissue margins was collected for histological studies.

2.14. Histolopathological examination

The dissected skin specimens were fixed in 10% neutral formalin, processed, embedded in paraffin, cross-sectioned and stained with hematoxylin-eosin or masson trichrome stain to study the wound closure properties. Histological photographs were performed in 5 µm tissue sections using a light microscope 211 Leica DM750 (Leica Microsystems GmbH, Germany) with an attached digital camera 212 Leica ICC50 HD (Leica Microsystems GmbH, Germany). A systematic examination of 40 random fields under 200X magnification was performed in order to semi-quantitatively score the following histological parameters: necrosis, inflammation, granulation tissue formation, angiogenesis, re-epithelization and collagen tissue deposit.

2.15. Statistical Analysis

All experiments were replicated three times; results are expressed as the standard error of the mean (SEM). Statistical analyses were performed using GraphPad Prism software (Version 9) by one-way ANOVA analysis of variance followed by Dunnett's or Šidák's multiple comparisons test. A two-way ANOVA test followed by Tukey's multiple comparisons was chosen to compare groups in the cell viability tests. $p<0.05$ was considered statistically significant.

3. Results and discussion

3.1. Peptide screening

The ability of short yeast-derived peptides to influence cytokine production by macrophages, fibroblast proliferation, collagen synthesis, cell migration, and microbial growth was investigated.

3.1.1. Physicochemical properties of peptides

To investigate the wound healing potential of yeast-derived peptides such as VLSTSFPPK (VL-9) and YGKPVAVPAR (YR-10) and their structural analogues, we evaluated several key properties, including their immunomodulatory, growth promoting and antimicrobial activities. Table 1 contains the amino acid sequence and theoretical features of the peptides. The molecular weight, isoelectric point (pI), and net charge at pH 7 were predicted using the Pepdraw tool (http://www.tulane.edu/biochem/WW/PepDraw/), and the GRAVY indexes were predicted using the Protparam tool (http://web.expasy.org/protparam). The positive and

negative values of the GRAVY index correspond to peptides' hydrophobic and hydrophilic properties, respectively. The molecular weight of the peptides ranged from 342.40 to 1137.31 Da. The isoelectric point ranged from 5.53 to 11.29.

Peptides	Sequence	Molecular weight (Da)	Net charge at pH 7	Theoretical isoelectric pH	GRAVY* index
VL-9	VLSTSFPPK	974.54	+1	9.80	0.156
VY-9	VLSTSFPPY	1009.51	0	5.53	0.444
VW-9	VLSTSFPPW	1032.52	0	5.58	0.489
(Modified VW-9)	(CTGVLSTSFPPW)	1293.60	0	5.29	0.483
VF-9	VLSTSFPPF	993.51	0	5.56	0.900
VCK-9	VLSTSFCPK	980.49	+1	8.67	0.611
VYK-9	VLSTSFYPK	893.48	+1	9.48	0.189
VHK-9	VLSTSFHPK	1014.54	+1	9.80	-0.022
SK-7	STSFPPK	768.32	+1	9.8	-0.943
YR-10	YGKPVAVPAR	1057.26	+2	10.41	-0.130
YHR-10	YGKHVAVHAR	1137.31	+2	10.41	-0.450
GA-8	GKPVAVPA	737.90	+1	10.2	0.562
GHA-8	GKHVAVHA	817.45	+1	10.12	0.163
PAR-3	PAR	342.40	+1	11.29	-

Table 1. The physicochemical properties of the peptides investigated in this study

The molecular weight, isoelectric point (pI), and net charge at pH 7 were predicted using the Pepdraw tool (https://pepdraw.com/), and the GRAVY (Grand average of hydrophobicity) indexes were predicted using the Protparam tool (http://web.expasy.org/protparam).

3.1.2. Peptides effect on macrophage and fibroblast viability

Using the CellTiter-Glo Luminescent cell viability test, we investigated the effect of different peptides concentrations (0.25, 0.5, and 1mM) on U937 and fibroblast viability after 24, 30, and 48 h of incubation at 37 °C.

None of the tested peptides showed significant cytotoxicity. However, during the first 30 h of cell culture, the peptides VL-9, VY-9, VW-9, VF-9, VCK-9, VHK-9, and VYK-9 significantly stimulated the growth of U937 and fibroblast ($p<0.05$) (Fig. 1A and 1B). Our finding confirmed the importance of peptide hydrophobicity on their proliferative effect since hydrophobic peptides were more effective on cell proliferation compared to hydrophilic peptides. Previous research also showed that the high content of hydrophobic amino acids promotes cell proliferation due to interaction with cells and modulating cell growth[27-29].

The results of comparing peptides for proliferation effect on U937 and fibroblasts showed that replacing Lys in the C-terminus of VL-9 with Trp and Phe increased the percent of cell proliferation, indicating a favorable role for Trp and Phe in the C-terminus of peptides VF-9 and VW-9 (Fig. 1C).

Finally, the most effective peptides for cell proliferation were VF-9 and VW-9. The low molecular weight (1 kDa) of VF-9 and VW-9 may be an important factor in peptide cell penetration, because earlier research has demonstrated that small-size peptides have increased proliferative activity on several cell lines [30, 31]. It could also possibly be owing to the hydrophobic nature of peptides and the presence of aromatic amino acids, Phe and Trp, at the C-terminus, as aromatic amino acids have previously been identified as essential factors in cell proliferation [32].

3.1.3. Immunomodulatory activity of peptides

The monocyte-derived macrophages were used as an *in vitro* model to investigate the inflammatory markers and macrophage activation by LPS and IFN-γ. LPS is detected by macrophages via specific receptors, primary Toll-like receptor complex, resulting in activation of signaling pathways mostly including NF-κB and MAPKs that leads to overexpression of genes and increased production of inflammatory cytokines such as TNF-α, IL-6 and IL-1β. IFN-γ is also a powerful macrophage activator that increases the cell ability to perform an immune response. The main pathway elicited by IFN-γ is the JAK-mediated phosphorylation of STAT1 that induces the expression of CD64 [33, 34]. Modulation of the production of inflammatory cytokines (TNF-α, IL-6, and IL-1β in LPS-treated macrophages and the surface expression of CD64 in IFN-γ-stimulated cells are two useful read-outs to evaluate the anti-inflammatory potential effects of these components.

As expected, LPS treatment induced cytokine production by U937 cells. The frequency of TNF-α^+ cells increased from 0.38% ± 0.01 to 24.3% ± 0.98 (Fig. 2A and 2B-I), MFI increased from 253 ± 3.8 to 424 ± 6.90 and TNF-α concentration in cell-free supernatant increased from under detectable level to 6196 ± 134.17 pg/mL (Fig. 2B-III). Furthermore, LPS treatment increased the concentrations of IL-6 in cell free supernatant from under detectable level to 596 ± 14.00 (Fig. 2B, IV). MFI value for CD64 of IFN-γ-stimulated cells increased from 21521 ± 3421 to 50216 ± 3170 (Fig. 2B, II).

TNF-α, IL-6, and CD64 levels in cells pretreated with the peptides and stimulated with LPS and IFN-γ were evaluated to assess their immunomodulatory activity. Flow cytometry and ELISA tests revealed that pre-treatment with VW-9 significantly modulated the capacity of cells to produce TNF-α. The proportion of TNF-α positive cells was reduced from 24.3 % ± 0.98 to 16.8% ± 1.03 (Fig.2A) and MFI values from 424 ± 6.90 to 351 ± 2.60. The levels of IL-6 also decreased by 44.75% ± 6.18 in cells pre-treated with VW-9 (Fig. 2B-IV). VW-9 was also effective in reducing the MFI value of CD64 positive cells by 17.50% ± 8.06 (Fig. 2B-II). Although U937 has been utilized in the literature as a model for considering the anti-inflammatory activity of compounds, there are some variations between receptors in U937 and macrophages, hence using primary macrophages extracted from rats is recommended for further research.

The structural and physicochemical properties of anti-inflammatory peptides have been poorly studied. Most anti-inflammatory peptides that have been reported in various research are small-sized peptides. For example anti-inflammatory peptides VPP and IPP resulting from bacterial fermentation of milk, IRW and IQW obtained from egg casein, and PAY isolated from salmon byproduct protein, and PTGADY from Alaska pollock protein [35] have a molecular weight

less than 1 kDa [36]. The exact relationship between peptide size and its anti-inflammatory activity is not well-established, but some reports attributed the higher anti-inflammatory of small-sized peptides to the easier absorbance by immune cells [37]. Peptides that penetrate cells usually have a sequence length of 5 to 42 amino acids [38]. The size of VW-9 may also have influenced its anti-inflammatory activity.

Acidic nature (pI= 5.58), the presence of hydrophobic amino acids, Val, Leu, and Pro, as well as aromatic amino acids Trp and Phe have been reported for several anti-inflammatory peptides [7, 39-41] and may also justify the higher anti-inflammatory effects of VW-9 in comparison to other peptides. In addition, our findings revealed that Trp is a key amino acid residue in C-terminus of anti-inflammatory peptides. It was discovered by comparing the activity of VL-9, VW-9, VF-9, and VY-9, all of which had similar sequences but a distinct C-terminus, including Lys, Trp, Phe, and Tyr, respectively. Trp was also previously found in the same place in the sequence of two anti-inflammatory peptides derived from egg protein, IRW and IQW [42, 43]. VW-9 peptide having the greatest inhibitory effect on TNF-α and IL-6 cytokines in LPS-stimulated cells and CD64 levels in IFN- γ stimulated cells was evaluated for anti-inflammatory mechanisms by evaluating its influence on regulation of the NF-B and p38 MAPk pathways and expression of anti and pro-inflammatory cytokines gene. We did not observe suppressing effects of the peptide on NF-κB and MAPK pathways based on phosphorylation and mRNA assays (Fig. S3). Inflammation is a complex immune response involving multi genes and cytokines [44]. Numerous processes would be studied to ascertain the precise mechanism underlying anti-inflammatory activity. Effect of the peptide on pro-inflammatory c-Jun N-terminal kinase (JNK, member of the MAPKinase family) pathway [45], inhibition of NO/iNOS and PGE2/COX-2 pathways [36], regulation of the STAT1/IRF3 signaling pathway [46], and regulation of PI3K/AKT pathway [47], destabilization of cytokine mRNA and action on post-transcriptional steps are among the other mechanisms that maybe involved in anti-inflammatory activity of VW-9 and more research is required to pinpoint the precise mechanism(s) of the anti-inflammatory activity of VW-9 [48].

3.1.4. In vitro wound scratch assay

The ability of the peptides to induce collagen production and fibroblast migration was investigated for a better understanding of their wound healing potential. We tested the collagen synthesis of the cells following incubation with 0.5 mM of the peptides for 24 h. Except for VYK-9, VHK-9, and SK-7, all other peptides significantly increased collagen production in fibroblasts (Fig.3I). VF-9, GHA-8, PAR-3 were the most effective peptides, which induced 111.59% ± 17.75, 108.24% ± 3.57, and 108.24 ± 9.44 increases in collagen production. VW-9 also effectively stimulated cells to produce 44.94% ± 6.24 more collagen.

Cell migration was also observed after 16 h in cells treated with VF-9, VW-9, and VYK-9 compared to the control (Fig. 3II and 3III).

The presence of Val and Leu at the N-terminus of the peptide was observed as a common feature of VL-9, VY-9, VW-9, and VF-9 (under investigation in this research) and VLPVPQK described by Kumar et al. [49] for fibroblast stimulating effect. In addition, SK-7 which has the same sequence as VL-9 but lacks Val and Leu at N-terminus, did not affect fibroblasts, demonstrating the important role of Val and Leu on fibroblast stimulation.

Our findings showed that the substitution of Lys with Phe in VL-9 resulted in a 40% increase in collagen formation, suggesting the more favorable impact of Phe as an aromatic hydrophobic amino acid in the C-terminus of peptides having a positive effect on fibroblasts than Lys. VL-9 and VCK-9 with Pro and Cys in the antepenultimate position had a greater influence on collagen formation compared to VYK-9 and VHK-9 with Tyr and His at the same position. These results indicate the beneficial role of Pro and Cys in the antepenultimate position of peptides for such effects. Pro was also reported in the antepenultimate position of VLPVPQK, a peptide previously reported for stimulating effect on fibroblasts [49].

The beneficial effect of VF-9 and VW-9 on fibroblast migration and collagen production demonstrates the beneficial role of aromatic amino acid in the C-terminus of peptides with fibroblast's stimulating effect and also confirms the previous findings on the critical role of peptide hydrophobicity in fibroblast's stimulation, as it results in improved peptide-cell interaction and a more modulatory effects [27, 28].

3.1.5. Antimicrobial activity

All synthetic peptides were tested for antimicrobial activity against two common skin pathogens, *E.coli* (ATCC 25922) and *Staphylococcus aureus* (ATCC 25923). Four of the 13 peptides tested, including GA-8, VHK-9, YR-10, and SK-7 demonstrated antimicrobial activity. GA-8 was found to be antimicrobial against both *E. coli* and *S. aureus*. GA-8's MIC and MBC against *E. coli* and *S. aureus* were 10 mM and 20 mM, respectively. VHK-9 and YR-10 were found to have antimicrobial activity against *S. aureus*, with MICs of 5 mM for both. SK-7 showed antimicrobial activity against *S. aureus*, with a MIC of 10 mM. None of the peptides studied in this research showed multifunctional immunomodulatory and antimicrobial activities (data are not shown).

Even though the structure-function relationship of antimicrobial peptides is poorly understood, it has been demonstrated that the mechanism of action is dependent on peptide type, microbial target, and experimental conditions [50]. It has been shown that membrane interaction is the most important component in peptide antimicrobial activity, regardless of whether the target is a membrane or intercellular compound [51]. Peptides with cationic property can interact electrostatically with anionic components of Gram-positive and Gram-negative bacterial cell membrane, causing membrane integrity to be disrupted and/or translocate across the membrane to the cytoplasm to act on intracellular targets [52]. Having both hydrophilic and hydrophobic domains is also a key element for interacting antimicrobial peptides with the target cytoplasmic membrane. The charged domain of peptide interacts with hydrophilic groups of phospholipids, while the hydrophobic domain interacts with the hydrophobic core of the lipid bilayer, forcing the peptide further into the membrane [51, 53, 54]. Aside from electric charges and peptide hydrophobicity, the type and sequence of amino acids play a role in antimicrobial action [55, 56].

3.2. Peptide-functionalized MEW scaffolds

PCL is the most widely used biocompatible, low-cost, biodegradable polymer for melt electro writing [57]. In the MEW method, an electrically charged, viscose polymer is sustained at a low flow rate from a nozzle using an applied voltage and collected on a glass collector, where the fibers form layer by layer structure.

VW-9 with the highest anti-inflammatory activity, proliferation effect on fibroblasts and macrophages, and fibroblast stimulating activity was investigated for functionalization of PCL polymer through two different pre- and post-functionalization strategies as described in material and methods section**.** The pre-functionalization strategy consists in blending the peptide and PCL before MEW. Weak interactions are established between the active molecule and the polymer. Although the contact between peptide and polymer is unstable, non-covalent physical interactions are notable for their simplicity and ease of active molecule release. [58]. On the contrary, the post-functionalization strategy involves covalent grafting of the peptide onto printed scaffolds. In CDI chemistry, the ester bonds of PCL are first partially aminolyzed with hexamethylene diamine (HMD) to generate nucleophilic amines on the PCL surface. Then amines from the HMD-treated PCL are coupled to the C-terminal carboxylic acid of the peptide activated by CDI, resulting in an amide bond between the peptide and the modified PCL (Fig. 4A). A modified VW-9 sequence with Cys (for grafting) and Tyr and Gly (as spacers) in the N-terminus was devised to accomplish peptide grafting using thiol chemistry. In thiol chemistry, PCL is chlorinated with CEA, and then the peptide is conjugated via substitution of chlorine by the thiol of the Cys residue of the peptide [12] (Fig. 4B). Polymer`s surface of some samples were plasma treated to generate hydrophilic moieties on PCL that aid in the establishment of hydrogen bonds with biomolecules, as well the cell attachment to the polymer surface [23, 58]. A list of different scaffolds investigated in this research is provided in Table 2.

Table 2. The name of the peptide-functionalized PCL and the procedures used to make them

Sample name	Grafting method	Plasma-treatment	reaction	Peptide sequence
A0 (native PCL)	-	-	-	-
A1	Post fabrication (Chemical reaction)	-	CDI chemistry	VLSTSFPPW (VW-9)
A2	Post fabrication (Chemical reaction)	+	-	-
A3	Post fabrication (Chemical reaction)	+	CDI chemistry	VLSTSFPPW (VW-9)
A4	Post fabrication (Chemical reaction)	-	Thiol chemistry	CTGVLSTSFPPW (Modified VW-9)
A5	Post fabrication (Chemical reaction)	+	Thiol chemistry	CTGVLSTSFPPW(Modified VW-9)
A6	Pre fabrication (Physical mixing)	-	-	VLSTSFPPW(VW-9)
A7	Pre fabrication (Physical mixing)	-	-	VLSTSFPPW (VW-9)
A8	Pre fabrication (Physical mixing)	-	-	VLSTSFPPW (VW-9)

3.2.1. Characterization of peptide-functionalized scaffolds

The XPS analysis of the scaffolds before and after plasma treatment (Fig. 4G) revealed an increase in the surface oxygen content from 22.2% ± 1.50 to 27.3% ± 1.70, thus confirming its favorable function in boosting the level of oxygen-containing functionalities on the scaffolds surface. In fact, argon plasma contains several non-reactive species such as excited atoms, photons, electrons, molecules, and ions that are capable of breaking surface C-H and C-C chemical bonds to generate radicals. Since no chemically reactive species are theoretically present in an Ar plasma, the formed surface radicals are only expected to interact with each other leading to cross-linking and double bond formations. Nonetheless, the working environment in the DBD is not entirely pure as oxygen impurities emerging from a contaminated Ar flow and air remaining inside the chamber are unavoidable. As such, these oxygen traces can react with the surface radicals leading to the implantation of oxygen-containing groups such as carboxyl (O-C=O), hydroxyl (C-O) and carbonyl (C=O) on the PCL surface. Moreover, post-plasma oxidation processes between atmospheric oxygen species and plasma-induced surface radicals can also occur [19]. SEM analysis of the scaffolds before and after plasma treatment (Fig. 4F) revealed that the plasma treatment caused no morphological damage to the scaffolds.

The FTIR spectra of A1 sample (CDI chemistry) showed the presence of amide A band (about 3500 cm^{-1}), amide B (about 3100 cm^{-1}) and amide I band (1600-1700 cm^{-1}). The spectra of A4 sample (Thiol chemistry) exhibited smaller peaks at the same wave numbers (Fig. 4C). These results suggested that VW-9 and modified VW-9 were successfully incorporated into PCL scaffolds and higher amounts of the peptide were grafted by CDI chemistry method compared to the thiol chemistry method. The FTIR spectra of the A7 sample were similar to that of PCL, which could be due to the small amount of peptides present or the non-homogeneous distribution of peptides on the scaffold surface or maybe because peptides are hidden inside the strunts of scaffolds.

Elemental analysis of Nitrogen in scaffold samples also revealed that CDI chemistry produced a greater value of grafted peptide (0.43% w/w) than thiol chemistry (0.026% w/w) and physical grafting method (0.016%). Plasma treatment did not increase the level of grafted peptide (0.4%) compared to the values (0.43%) in non treated PCL.

As illustrated in Fig. 5, the morphology of scaffold fibers was smooth, uniform, and bead-free. Across all scaffold groups prepared by covalent bounding of peptide (post fabrication method), fiber dimeters ranged from 31.6±0.84 µm to 33.61±1.28 µm (N=5 scaffolds per group). Pre functionalization method for fabrication of peptide-functionalized scaffold generated significant alterations in the structure and size of fibers. Increasing the peptide content from 0.25% to 2% w/w resulted in a noticeable shift in the scaffold structure. In addition, most of the PCL struts were thinner than when pure PCL was used . Other researchers also reported scaffolds created through pre functionalization strategy, with mixing Lactoferrin (0.25%) and a combination of Lactoferrin and whey protein (0.25%) with PCL had thinner struts than scaffolds made with PCL alone [5]. SEM pictures of A1, A2, and A3 also revealed the presence of peptides on the scaffold surface. Although, it was not visible on other samples (Fig. 5).

Following streptavidin labeling, fluorescent examination of grafted peptides was carried out (Fig. 6). The increased fluorescence intensity in sample A3 compared to A1 demonstrated the influence of plasma treatment on increased reactivity of PCL scaffold with peptide via CDI chemistry. More carboxylic acid groups are activated on the surface as a result of plasma treatment, which is then activated with EDC and NHS and coupled to peptide [59].

The higher fluorescence intensity assessed for A1 and A3 when compared to other samples created using thiol chemistry, as well as physical interaction, validated our previous findings that CDI chemistry was more successful in grafting a larger amount of peptide.
In addition, the stability of the peptide in the structure of the peptide-functionalized scaffold was examined when it was exposed to heat (95°C) during the printing process, as part of a post-fabrication strategy that might last up to 6 h. The LC/MS spectra of peptide VW-9 acquired before and after heating (Fig. 4E) were identical, and no new peaks arose on the UV or SIR signal after heating at 95°C, indicating that the peptide is stable at this temperature for 6 h. UPLC/MS quantification of the peptide released from pre-functionalized scaffolds that roughly 5% of the total added peptide was released during the first 8 h of incubation at 37°C in PBS solution, and then remained stable for the next 24 h (Fig. 4D).

3.2.2. Cell behavior on the surface of functionalized scaffolds

Cell adhesion and growth on biomaterial surfaces are dependent on cell-material interactions. The immobilization of biomolecules on scaffold surfaces may improve cell responsiveness [12]. Cell adhesion is a critical process in the development of multicellular organisms. Cell adhesion occurs due to the interaction of support with the cell adhesion receptors, which leads to remodeling of the cytoskeletal filaments supporting the cell shape and the spreading of cells on support [60].

3.2.2.1. Cell viability

Porous scaffolds provide a physical surface for cells to adhere and provide a favorable environment for cell proliferation and growth. The porous aspect of the scaffold allows for consistent delivery of nutrients and oxygen to the skin cells [1]. An ideal porous scaffold has a specific pore size with increased porosity and an optimum surface to volume ratio that enables the diffusion of nutrients and mimics the natural environment for cell growth [61]. The cell viability on PCL porous scaffold pretreated with plasma and functionalized with peptide was evaluated and compared with native PCL scaffold (A0).
Functionalization of PCL scaffolds with peptides through CDI chemistry (A1) promoted fibroblast proliferation but was not effective for macrophages (Fig. 7A-I and 7B-I**).** Plasma treatment (A2) alone increased the proliferation of macrophages, significantly. The combination of plasma treatment and peptide grafting (CDI chemistry) (A3) increased both macrophages (after 24 and 48 h) and fibroblasts viability (after 24 h) compared to native PCL (A0). The combined effect of plasma and peptide on macrophage proliferation was considerably ($P<0.05$) greater than either plasma or peptide alone (Fig. 7A-I and 7 B-I).
The functionalization of PCL scaffolds with peptide by thiol chemistry (A4) did not increase macrophage and fibroblast proliferation, however the combination impact of plasma and peptide (A5) induced an increase in macrophage and fibroblast proliferation after 48 h (Fig.7A-II and 7B-II).
Physical incorporation of peptides in the scaffolds was only efficient at a concentration of 1% (w/w) to increase the proliferation of fibroblasts after 7 days (Fig. 7A-III and 7B-III). This observation can be attributed to low peptide concentrations as well as peptide burying in the fibers, which renders them biologically unavailable to the target cell population [62]. Despite the lack of an effect on cell proliferation, the data revealed that macrophages and fibroblasts

are at least as viable on physically modified scaffolds as they are on native PCL, and these scaffolds are also appropriate substrates for cell growth.

3.2.2.2. Cell distribution and morphology

Scaffolds play a unique role in repair and regeneration of tissues by providing a suitable platform, permitting an essential supply of factors associated with the survival and adhesion of cells [63]. The adherent cell distribution and morphology on peptide-functionalized PCL were studied using wide field fluorescence microscopy pictures and SEM analysis after culturing PMA-treated U937 cells and fibroblasts on the scaffold's surface.

Considering the morphology of cells on the aligned fibers of scaffolds, shows their growth and spreading parallel to the fibers. Porous structure of scaffolds also prevented cells from clumping and formation of necrotic centers [1]

By comparing the cell density and distribution on fluorescence images of samples A0, A2, and A3, which were chosen based on viability experiment findings, we established that the macrophage cell population density is substantially higher on plasma treated samples (A2) than on A0. Argon plasma discharges will probably add oxygen-containing groups such as OH, C=O, and C-O groups on the scaffold. These incorporated functional groups enhanced cellular adhesion, proliferation and growth due to higher wettability of plasma treated scaffolds [64]. The combination effect of plasma and peptide (A3) increased the density of the macrophage population compared to either native PCL (A0) and plasma treated (A2) samples (Fig. 8).

For fibroblasts, however, an increase in cellular density was detected on plasma-treated samples but combining plasma and peptide grafting did not cause further improvement in cell population (Fig. 8).

There is a substantial link between cell shape, spreading behavior, and surface characteristics [65]. SEM images did not show a discernable difference in macrophage morphology and spreading behavior between post-functionalized (A1-5) and native PCL scaffolds (A0). However, when compared to post-functionalized scaffolds, the cell shape on scaffold A7 was more rounded with a very short axis and a smaller interfacial contact area and no well-developed lamelliopodial extensions (Fig. 9). The post-functionalization technique may influence the surface topography and roughness of the polymer, which in turn affects macrophage adhesion to the surface of the scaffold [66, 67].

Representative pictures of fibroblasts revealed that these cells spread well on both native and peptide-functionalized PCL (Fig. 10).

3.2.2.3. Anti-inflammatory activity of peptide-functionalized scaffolds

In constructing wound healing scaffolds, one interesting strategy has been to modify synthetic biomaterial molecules with biological features such as anti-inflammatory activity [63].

Our findings (Fig. 11) revealed that all peptide-functionalized PCL had varying degrees of anti-inflammatory efficacy, with A3 and A5 showing the most. Although, peptide grafting (A1 and A4) and plasma treatment of scaffolds (A2) alone resulted in a lower inflammatory response than A0, the combination of plasma treatment with peptide grafting by both CDI (A3) and thiol chemistry (A5) resulted in the highest anti-inflammatory activity.

Two distinct aspects including grafted peptide quantity and activity as well as scaffold surface features contribute to the anti-inflammatory efficacy of peptide-functionalized PCL. The anti-

inflammatory activity of grafted peptide, however, influenced by the type of interaction, the amino acids involved in interaction and orientation of peptide after grafting. For example, the conformation of the absorbed peptide can be changed on hydrophobic PCL due to hydrophobic interactions between surface and hydrophobic peptide. Such absorption and conformation change may affect subsequent cellular inflammatory response.

After CDI chemistry, the amine group on the polymer is engaged in an amine bond with the carboxylic acid on the peptide C-terminus. It means that the Trp in VW-9's C-terminus is engaged in PCL interaction. However, the CDI chemistry is not a chemo selective reaction. The free amino groups of Lys, the free N-terminus of the peptide, and the hydroxyl groups of Ser and Thr may cause unspecific and undesired intramolecular and intermolecular peptide conjugation. Peptide activation at the C-terminus can also lead to peptide epimerization [58]. But thiol chemistry is a chemo selective reaction in which the chlorine atom on chlorinated PCL is substituted by the thiol of the Cys residue in N-terminus of modified peptide [12, 68]. Tyr and Gly operate as spacers in the sequence of modified VW-9, ensuring appropriate display of the peptied on the surface to enable interactions with cells [58]. In contrast to CDI chemistry, the Trp in the peptide C-terminus, which is known as a key amino acid implicated in the peptide anti-inflammatory function, is not engaged in a covalent bond with the polymer which makes Trp available for interaction with cells [42, 43]. The chemo selectivity of the thiol process could explain why A4 has stronger anti-inflammatory efficacy than A1.

On the other hand, the surface chemistry of functionalized biomaterials impacts wettability, charge density, protein and cell adsorption and subsequent cellular behavior [69]. Many studies have shown that the inflammatory responses of different scaffolds are highly a surface dependent property [66, 70]. The increased anti-inflammatory activity of plasma-treated samples (A2) compared to non-treated scaffold (A0) could be attributed to the hydrophilic property of plasma-treated samples. Because hydrophobic surfaces have been found to promote inflammatory reactions with increasing adhesion, macrophage fusion, and pro-inflammatory cytokine release, hydrophilic surface exhibits anti-inflammatory activity with inhibition of macrophage fusion and pro-inflammatory cytokine production [69].

Although the post-fabrication procedure produced a modest amount of grafted peptide, anti-inflammatory tests revealed that cells cultured on the surface of the A7 scaffold produced less TNF-a and IL-6 cytokines than cells cultured on the surface of the A0 sample. The lower production of inflammatory cytokines can be attributed to the peptide's anti-inflammatory effect as well as decreased cytokine release as a result of alterations in the scaffold structure, which alters macrophage adhesion and infusion as well as cytokine secretion levels [66].

3.2.2.4.In vivo wound healing potential of free and grafted peptide VW-9

Next, an in vivo preclinical model divided in two categories, was carried out to investigate first the effect of bare peptide VW-9 solution and then of the peptide-functionalized PCL scaffold on wound healing using full-thickness excisional wounds created on rat skin.

First, the *in vivo* study of wound healing profiles for the two treatments, namely PRP solution (Platelet-Rich Plasma, as the positive control) and peptide solution, and their controls were illustrated in Fig. 12A. The results of wound healing ratio during the wound healing process were exemplified in Fig.12C. PRP was considered positive control for the first part of the study, since it was used in the solution form as the peptide, and is recognized to directly enhance

healing by local release of growth factors, cytokines, as well as inflammatory mediators, essential for complete regeneration [71]. No sign of edema, erythema or suppuration in the wound area was observed on the treated groups over the 7 experimental days, suggesting that a regular course of wound healing was promoted. The results showed that both PRP and VW-9 solutions significantly reduced the wound area compared to the control wound region ($p<0.05$).

On day 3 of the study, the wounds showed similar characteristics for the two experimental groups, as there was no significant difference in the wound size between the treated groups and control, 26.81±9.99% and 20.44±3.84% for the PRP and the VW-9 treated groups respectively. On day 5, the PRP group seemed to be better (47.56± 5.02%) in promoting wound healing than the VW-9 (44±3.77%), as seen in the visual comparisons from Fig. 12A. As observed, the wound area of the control groups has significantly (28 ±5.02%) decreased at day 5.

On the 7th day, the percentage of wounds healing in the PRP and VW-9 groups reached nearly 70% and a significant difference ($p<0.05$) was observed for both PRP and VW-9 treated wounds when compared with their respective controls (Fig. 12C).

The second part of the *in vivo* experiment followed the effect of the grafted peptide VW-9 onto PCL scaffold and of a similar in texture commercial dressing, Sorbalgon® that contains calcium alginate. Also, the negative control was added for each animal, where the wounds were left untreated and only covered with cotton gauze. As can be seen in Fig.12D**,** the rat wounds covered with peptide-loaded PCL scaffolds exhibited an accelerated wound closure at day 12 and 16 as compared with the rats treated with Sorbalgon® and the untreated control wounds. In the first 4 days, both scaffolds (peptide based and commercial) adhered well on the wound surface, and there seemed to be 4.5 % difference in the healing rates, and nearly 8.5 % variation when compared with the negative control. On the 8th day, all the wound areas maintained relatively the same look as observed in Fig. 12D, but with a higher (nearly 3 or 6 %, respectively) wound healing rate for the tested scaffold as compared with the control groups. At the next evaluation (at 12th day), the wounds treated by the peptide scaffold presented an 80.23 ± 5.31% wound closure, higher than that of group C+ (72.55 ± 1.84%), while the healing rate of the blank control (C-) was only 66.67 ± 13.86% ($p < 0.05$). At 16th day postoperatively, the results showed that the wound area of the tested group was significantly reduced, with 86.27 ± 0.51 % wound closure rate, whereas the one for the positive control group was 79.41 ± 0.66% and 81.70 ± 1.84% ($p < 0.001$), for negative control group. The quantitative analysis shown in Fig. 12F further reveals this trend.

3.2.2.5.The histopathological observations

Histological evaluation with H&E or Masson trichrome staining shown in Fig. 12 B and Fig. 12E**,** were exemplified for wound sections at days 3, 4, 7, 8, 12 and 16. Results exhibited that the healing conditions of the tested groups were better than that of the control groups in the specimen on day 7 for bare peptide VW-9 solution and day 12, respectively, for grafted peptide VW-9 onto PCL scaffold.

In the case of bare peptide VW-9 solution, on day 3, the wounds of the control groups present significant areas of necrosis and leukocyte exudation processes that replace the epidermis and partially destroyed dermis. In the PRP group, the wound is covered by a meshwork of fibrin, necrotic epithelial cells and neutrophils, and the dermis is invaded by severe congestion and a

leukocyte-rich fibrin infiltrate. Although some inflammatory cells were noticeable in the dermis, the necrotic and fibrinous material rich in mononuclear cells could also be observed at the superficial level.

At the VW-9 wound surface, an important fibrino-necrotic material, infiltrated with neutrophils, substitutes the damaged epidermis. At the dermis level, the inflammatory process is present, but more faded than in the PRP and control groups. Also, the cellular and fibrinous exudations are much lower, with less pronounced congestion, reduced edema, significant fibrinous exudation and reduced leukocyte influx. The condensed inflammatory cells (rare macrophages and fibroblasts) identified in the tissue matrix were resumed to microcirculation congestion and diffuse edema.

The wound sections on day 7 showed more pronounced differences between batches. As expected, the control groups are still in the inflammatory phase of healing. The intense inflammatory process is characterized by edema with significant leukocyte exudation. However, regarding re-epithelialization of the lesions treated with only ultrapure water present, it is clear that the keratinocytes layer is absent on the surface. In the wounds treated with PRP solution, a minor necrosis area could be observed, along with connective tissue neogenesis (fibroblasts and collagen fibers) and neoformation blood vessels. The newly formed scar tissue is loose and immature, suggesting reduced proliferation of keratinized stratified squamous epithelium (reduced re-epithelialization). On the contrary, in the lesions treated with the peptide solution, the re-epithelialization is mature with semi-oriented, dense young connective tissue, new covering epithelium resulting from the proliferation of keratinocytes at the edge of the wounds extending over the unformed one, demonstrating that the healing process is accelerated. More, a high number of blood vessels can be identified in the wounds treated with VW-9, indicating that peptide solutions strongly promote angiogenesis in vivo.

In the second part of the experiment, Masson's Trichrome staining was used to visualize connective tissues after the application of the peptide-based PCL scaffolds. On day 4, the negative control wounds show existing acute edema and moderate inflammatory infiltrate, but with significant necrosis and fibrinous exudation. The Sorbalgon® presence determined also an increased inflammatory edema, with its accumulation among degenerated collagen fibers. Even if the inflammatory infiltrate is moderate, the area of necrosis is accentuated, and the proliferation of fibroblasts and collagen fibers is absent. As expected, based on the bare peptide effect at the first monitorisation time-point, the scaffold determined a more limited necrosis area, but also with intensified inflammatory infiltrate and moderate inflammatory edema. As observed, the fibrinous exudation is present into the wound area, along with accentuated neogenesis of the collagen fibers.

At day 8, the epidermis of the negative control group (C-) was replaced by a fibrin-necrotic area infiltrated with inflammatory cells. The tendency of re-epithelialization is reduced, almost absent, with moderate congestion, fibrillar and vascular neogenesis. The commercial scaffold determined severe inflammatory edema and cell infiltrate, associated with significant conjunctival hyperplasia. Also, some positive outcomes were also observed, namely moderate congestion, neogenesis of collagen fibers and well-represented blood neoformation vessels. Even if the wound area of the bare peptide group was almost closed after 7 day (first part of the study), in the case of tested scaffold significant regeneration of the dermis through intense proliferation of fibroblasts and collagen fibers were observed. Also, important vascular

neogenesis, inflammatory infiltrate and important cell differentiation were the main events at this time-point.

The experiment continued, therefore at day 12, the wound healing scenario changes significantly for all batches. The negative control group presented moderate inflammatory edema, significant proliferation of fibroblasts and collagen fibers, capillary neogenesis and congestion. The area of the crust was formed of devitalized tissue and significant fibrinous exudation, and the periphery lesion area still presented inflammation, with a persistent necrosis on the surface. Unfortunately, the positive control wound area still presented superficial necrosis, numerous inflammatory cells and severe congestion. The tested scaffold continued its positive path, with the following events: Mmedium intensity inflammatory process, important fibrillar and vascular neogenesis, onset of re-epithelialization by the proliferation of epidermis epithelial cells.

At day 16, the negative control wounds showed prominent dermal connective bud, consisting of young connective fibers, slightly disorganized and infiltrated with inflammatory cells and moderate congestion. At this time-point, the superficial necrotic tissues were removed, the re-epithelialization process appeared discretely, but with important vascular neogenesis. The wound area of the positive control still presented a significant area of necrosis and marked inflammatory infiltrate in the centre of the lesion (dermis), but the proliferation of cells in the basal layer of the epidermis materialised with their arrangement on the surface of unformed connective tissue. The connective tissues in the dermis were represented by young collagen fibers that are being reshaped. Intense epithelialization noted by proliferation of cells in the basal layer of the epidermis at the periphery of the lesion, was observed in the wounds treated with the tested scaffolds. Also, the congestion was present with moderate inflammatory infiltrate. The connective tissue are maturing and organizing, but the unformed connective fibers are still slightly disordered.

The level of wound closure was indicated also, by using scoring of histological parameters from minimal-to-very intense or complete appearance. The wounds treated with aqueous peptide fraction showed better histologic scores than PRP and control wounds, as shown in Table 3. Similar scores were observed also for the PCL scaffold group in comparison with the positive and negative controls, assessment presented in Table 4.

Table. 3. Semi-quantitative evaluation of histological parameters for the assessment of wound healing by using bare peptide VW-9 solution. Notes: + mild; ++ moderate; +++ extensive; ++++ very intense; − absence.

Histological parameters	Day 3			Day 7		
	Control	PRP	VW-9	Control	PRP	VW-9
Necrosis	+++	+++	+++	+++	+	-
Congestion	+++++	+++++	+++++	+++	+	+
Inflammatory edema	+	+	+++	++++	-	-
Fibrinous exudation	+++++	+++++	+++	++++	-	-
Leukocyte infiltrate (neutrophils, macrophages, lymphocytes, histiocytes)	+++++	+++++	+++	++++	++	+
Resorption of the fibrinous matrix	-	-	-	+	++++	+++++
Cell differentiation in the wound (endothelial cells, fibroblasts)	-	-	-		++++	+++++
Fibrillar neogenesis (collagen fibers) and neoformation of blood vessels	-			++	++++	+++++
Re-epithelialization	-	-	-	+	++	+++

Table 4. Semi-quantitative evaluation of histological parameters for the assessment of wound healing by using peptide-functionalized PCL dressing. Notes: + mild; ++ moderate; +++ extensive; ++++ very intense; − absence.

Histological parameters	Day 4			Day 8			Day 12			Day 16		
	C-	C+	T	C-	C+	T	C-	C+	T	C-	C+	T
Necrosis	+++	+++	++	+++	+++	+	++	+++	-	-	+++	-
Congestion	+	+	++	++	++	++	+++	+++	++	++	++	+++
Inflammatory edema	+++	+++	++	++	+++	-	++	-	-	-	-	-
Fibrinous exudation	+++	+++	++	+++	++	+	+	++	-	-	-	-
Leukocyte infiltrate (neutrophils, macrophages, lymphocytes, histiocytes)	++	+	+++	+++	+++	+++	+++	+++	+	+++	+++	++
Resorption of the fibrinous matrix	-	-	+++	-	-	+++	+	-	+++	+++	-	+++
Cell differentiation in the wound (endothelial cells, fibroblasts)	+	+	+++	++	+++	+++	++	+++	+++	++	++	+
Fibrillar neogenesis (collagen fibers) and neoformation of blood vessels	+	+	+++	++	+++	+++	+++	+++	+++	+++	++	+
Re-epithelialization	-	-	-	-	-	+	-	-	+	+	+	+++

4. Conclusion

We studied the effects of thirteen short yeast derived peptides with antioxidant activity on proliferation and stimulation of macrophages and fibroblasts, as well as their antimicrobial and anti-inflammatory activity, to assess their wound healing potential. In vitro and in vivo tests verified the wound healing characteristics of VLSTSFPPW (VW-9) and its potential to functionalize wound healing biomaterials. For the functionalization of a highly porous PCL scaffold generated by the melt-electrowriting process by VW-9, two alternative pre- and post-functionalization approaches were used, combining physical and chemical (CDI and thiol) coupling reactions with plasma treatment. The scaffold created by grafting peptide on the surface of the plasma-treated PCL scaffold using CDI chemistry demonstrated the highest in vitro and in vivo wound healing property.

Acknowledgment

This project has received funding from the European Union`s Horizon 2020 research and innovation programme under the Marie Sktodowska-Curie grant agreement No 801505. Authors likes to appreciate Dr. Louise Conrard, lab manager for microscopy, center for Microbiology and Molecular Imaging (CMMI) for her kind cooperation in microscopic analysis and Dr. Farzaneh Aziz - Mohseni, the head of Persian Type Culture Collection (PTCC) of Iranian Research Organization For Science and Technology (IROST) for providing microbial strains used in this study. Graphical abstract adapted from " Fibrotic Heart In Vitro Modelling", by BioRender.com (2022). Retrieved from https://app.biorender.com/biorender-templates.

Conflict of interest

The authors declare that they have no known competing financial interests or personal relationships that could have appeared to influence the work reported in this paper.

References

[1] A.A. Chaudhari, K. Vig, D.R. Baganizi, R. Sahu, S. Dixit, V. Dennis, S.R. Singh, S.R. Pillai, Future Prospects for Scaffolding Methods and Biomaterials in Skin Tissue Engineering: A Review, Int J Mol Sci 17(12) (2016).

[2] N. Paxton, S. Ho, B. Tuten, J. Lipton- Duffin, M. Woodruff, Degradation of Melt Electrowritten PCL Scaffolds Following Melt Processing and Plasma Surface Treatment, Macromolecular Rapid Communications 42 (2021).

[3] P. Feng, M. Liu, S. Peng, S. Bin, Z. Zhao, C. Shuai, Polydopamine modified polycaprolactone powder for fabrication bone scaffold owing intrinsic bioactivity, Journal of Materials Research and Technology 15 (2021) 3375-3385.

[4] N.E. Zander, J.A. Orlicki, A.M. Rawlett, T.P. Beebe, Quantification of Protein Incorporated into Electrospun Polycaprolactone Tissue Engineering Scaffolds, ACS Applied Materials & Interfaces 4(4) (2012) 2074-2081.
[5] E. Hewitt, S. Mros, M. McConnell, J.D. Cabral, A. Ali, Melt-electrowriting with novel milk protein/PCL biomaterials for skin regeneration, Biomed Mater 14(5) (2019) 055013.
[6] M. Nieuwoudt, I. Woods, K.F. Eichholz, C. Martins, K. McSweeney, N. Shen, D.A. Hoey, Functionalization of Electrospun Polycaprolactone Scaffolds with Matrix-Binding Osteocyte-Derived Extracellular Vesicles Promotes Osteoblastic Differentiation and Mineralization, Ann Biomed Eng 49(12) (2021) 3621-3635.
[7] M. Chalamaiah, W. Yu, J. Wu, Immunomodulatory and anticancer protein hydrolysates (peptides) from food proteins: A review, Food Chemistry 245 (2018) 205-222.
[8] M.L. Mangoni, A.M. McDermott, M. Zasloff, Antimicrobial peptides and wound healing: biological and therapeutic considerations, Experimental Dermatology 25(3) (2016) 167-73.
[9] M. Dadar, Y. Shahali, S. Chakraborty, M. Prasad, F. Tahoori, R. Tiwari, K. Dhama, Anti-inflammatory peptides: current knowledge and promising prospects, Inflammation Research 68 (2019) 125-145.
[10] P. Camacho, H. Busari, K.B. Seims, P. Schwarzenberg, H.L. Dailey, L.W. Chow, 3D printing with peptide–polymer conjugates for single-step fabrication of spatially functionalized scaffolds, Biomaterials Science 7(10) (2019) 4237-4247.
[11] P. Campagnolo, A.J. Gormley, L.W. Chow, A.G. Guex, P.A. Parmar, J.L. Puetzer, J.A.M. Steele, A. Breant, P. Madeddu, M.M. Stevens, Pericyte Seeded Dual Peptide Scaffold with Improved Endothelialization for Vascular Graft Tissue Engineering, Advanced Healthcare Materials 5(23) (2016) 3046-3055.
[12] A.C. de Luca, J.S. Stevens, S.L. Schroeder, J.B. Guilbaud, A. Saiani, S. Downes, G. Terenghi, Immobilization of cell-binding peptides on poly-ε-caprolactone film surface to biomimic the peripheral nervous system, J Biomed Mater Res A 101(2) (2013) 491-501.
[13] M. Mirzaei, S. Mirdamadi, M.R. Ehsani, M. Aminlari, Production of antioxidant and ACE-inhibitory peptides from Kluyveromyces marxianus protein hydrolysates: Purification and molecular docking, Journal of Food and Drug Analysis 26(2) (2018) 696-705.
[14] M. Mirzaei, S. Mirdamadi, M.R. Ehsani, M. Aminlari, E. Hosseini, Purification and identification of antioxidant and ACE-inhibitory peptide from Saccharomyces cerevisiae protein hydrolysate, Journal of Functional Foods 19 (2015) 259-268.
[15] M. Mirzaei, S. Mirdamadi, M. Safavi, Antioxidant activity and protective effects of Saccharomyces cerevisiae peptide fractions against H2O2-induced oxidative stress in Caco-2 cells, Journal of Food Measurement and Characterization 13(4) (2019) 2654-2662.
[16] L. Zhang, X. Wei, R. Zhang, J.N. Petitte, D. Si, Z. Li, J. Cheng, M. Du, Design and Development of a Novel Peptide for Treating Intestinal Inflammation, Frontiers in Immunology 10 (2019).
[17] M. Dadar, Y. Shahali, S. Chakraborty, M. Prasad, F. Tahoori, R. Tiwari, K. Dhama, Antiinflammatory peptides: current knowledge and promising prospects, Inflammation Research 68(2) (2019) 125-145.
[18] E.A. Barbosa, A. Oliveira, A. Plácido, R. Socodato, C.C. Portugal, A.C. Mafud, A.S. Ombredane, D.C. Moreira, N. Vale, L.J. Bessa, G.A. Joanitti, C. Alves, P. Gomes, C. Delerue-Matos, Y.P. Mascarenhas, M.M. Marani, J.B. Relvas, M. Pintado, J. Leite, Structure and function of a novel antioxidant peptide from the skin of tropical frogs, Free Radic Biol Med 115 (2018) 68-79.
[19] R. Ghobeira, C. Philips, L. Liefooghe, M. Verdonck, M. Asadian, P. Cools, H. Declercq, W.H. De Vos, N. De Geyter, R. Morent, Synergetic effect of electrospun PCL fiber size, orientation and plasma-modified surface chemistry on stem cell behavior, Applied Surface Science 485 (2019) 204-221.

[20] P. Camacho, M. Fainor, K.B. Seims, J.W. Tolbert, L.W. Chow, Fabricating spatially functionalized 3D-printed scaffolds for osteochondral tissue engineering, J Biol Methods 8(1) (2021) e146-e146.
[21] A.N. Hoofnagle, J.R. Whiteaker, S.A. Carr, E. Kuhn, T. Liu, S.A. Massoni, S.N. Thomas, R.R. Townsend, L.J. Zimmerman, E. Boja, J. Chen, D.L. Crimmins, S.R. Davies, Y. Gao, T.R. Hiltke, K.A. Ketchum, C.R. Kinsinger, M. Mesri, M.R. Meyer, W.J. Qian, R.M. Schoenherr, M.G. Scott, T. Shi, G.R. Whiteley, J.A. Wrobel, C. Wu, B.L. Ackermann, R. Aebersold, D.R. Barnidge, D.M. Bunk, N. Clarke, J.B. Fishman, R.P. Grant, U. Kusebauch, M.M. Kushnir, M.S. Lowenthal, R.L. Moritz, H. Neubert, S.D. Patterson, A.L. Rockwood, J. Rogers, R.J. Singh, J.E. Van Eyk, S.H. Wong, S. Zhang, D.W. Chan, X. Chen, M.J. Ellis, D.C. Liebler, K.D. Rodland, H. Rodriguez, R.D. Smith, Z. Zhang, H. Zhang, A.G. Paulovich, Recommendations for the Generation, Quantification, Storage, and Handling of Peptides Used for Mass Spectrometry-Based Assays, Clin Chem 62(1) (2016) 48-69.
[22] I. Alimov, S. Menon, N. Cochran, R. Maher, Q. Wang, J. Alford, J.B. Concannon, Z. Yang, E. Harrington, L. Llamas, A. Lindeman, G. Hoffman, T. Schuhmann, C. Russ, J. Reece-Hoyes, S.M. Canham, X. Cai, Bile acid analogues are activators of pyrin inflammasome, J Biol Chem 294(10) (2019) 3359-3366.
[23] M. Domingos, F. Intranuovo, A. Gloria, R. Gristina, L. Ambrosio, P.J. Bártolo, P. Favia, Improved osteoblast cell affinity on plasma-modified 3-D extruded PCL scaffolds, Acta Biomaterialia 9(4) (2013) 5997-6005.
[24] J.J. Martínez-Sanmiguel, G.Z.-T. D, R. Hernandez-Delgadillo, A.L. Giraldo-Betancur, N. Pineda-Aguilar, S.A. Galindo-Rodríguez, M.A. Franco-Molina, S.P. Hernández-Martínez, C. Rodríguez-Padilla, Anti-inflammatory and antimicrobial activity of bioactive hydroxyapatite/silver nanocomposites, J Biomater Appl 33(10) (2019) 1314-1326.
[25] H.-J. Park, M. Salem, A. Semlali, K.P. Leung, M. Rouabhia, Antimicrobial peptide KSL-W promotes gingival fibroblast healing properties in vitro, Peptides 93 (2017) 33-43.
[26] R.M. Humphries, J. Ambler, S.L. Mitchell, M. Castanheira, T. Dingle, J.A. Hindler, L. Koeth, K. Sei, C.M. Development, T. Standardization Working Group of the Subcommittee on Antimicrobial Susceptibility, CLSI Methods Development and Standardization Working Group Best Practices for Evaluation of Antimicrobial Susceptibility Tests, J Clin Microbiol 56(4) (2018) e01934-17.
[27] S. Benjakul, S. Karnjanapratum, W. Visessanguan, Hydrolysed collagen from Lates calcarifer skin: its acute toxicity and impact on cell proliferation and collagen production of fibroblasts, International Journal of Food Science & Technology 53(8) (2018) 1871-1879.
[28] C. Ozaki, S. Somamoto, S. Kawabata, Y. Tabata, Effect of an artificial silk elastin-like protein on the migration and collagen production of mouse fibroblasts, Journal of Biomaterials Science, Polymer Edition 25(12) (2014) 1266-1277.
[29] H. Ohara, S. Ichikawa, H. Matsumoto, M. Akiyama, N. Fujimoto, T. Kobayashi, S. Tajima, Collagen-derived dipeptide, proline-hydroxyproline, stimulates cell proliferation and hyaluronic acid synthesis in cultured human dermal fibroblasts, The Journal of Dermatology 37(4) (2010) 330-338.
[30] M. Lu, X.-H. Zhao, The growth proliferation, apoptotic prevention, and differentiation induction of the gelatin hydrolysates from three sources to human fetal osteoblasts (hFOB 1.19 Cells), Molecules 23(6) (2018) 1287.
[31] J. Wang, B. Zhang, W. Lu, J. Liu, W. Zhang, Y. Wang, M. Ma, X. Cao, Y. Guo, Cell Proliferation Stimulation Ability and Osteogenic Activity of Low Molecular Weight Peptides Derived from Bovine Gelatin Hydrolysates, Journal of Agricultural and Food Chemistry 68(29) (2020) 7630-7640.

[32] A. Jacquot, S.F. Gauthier, R. Drouin, Y. Boutin, Proliferative effects of synthetic peptides from β-lactoglobulin and α-lactalbumin on murine splenocytes, International Dairy Journal 20(8) (2010) 514-521.
[33] A.V. Villarino, Y. Kanno, J.R. Ferdinand, J.J. O'Shea, Mechanisms of Jak/STAT signaling in immunity and disease, J Immunol 194(1) (2015) 21-27.
[34] K. Kårehed, A. Dimberg, S. Dahl, K. Nilsson, F. Öberg, IFN-γ-induced upregulation of Fcγ-receptor-I during activation of monocytic cells requires the PKR and NFκB pathways, Molecular Immunology 44(4) (2007) 615-624.
[35] H. Hou, Y. Fan, S. Wang, L. Si, B. Li, Immunomodulatory activity of Alaska pollock hydrolysates obtained by glutamic acid biosensor – Artificial neural network and the identification of its active central fragment, Journal of Functional Foods 24 (2016) 37-47.
[36] C.B. Ahn, Y.S. Cho, J.Y. Je, Purification and anti-inflammatory action of tripeptide from salmon pectoral fin byproduct protein hydrolysate, Food Chem 168 (2015) 151-6.
[37] Z. Shi, B. Dun, Z. Wei, C. Liu, J. Tian, G. Ren, Y. Yao, Peptides Released from Extruded Adzuki Bean Protein through Simulated Gastrointestinal Digestion Exhibit Anti-inflammatory Activity, Journal of Agricultural and Food Chemistry 69(25) (2021) 7028-7036.
[38] E.C.L. de Oliveira, K. Santana, L. Josino, A.H. Lima e Lima, C. de Souza de Sales Júnior, Predicting cell-penetrating peptides using machine learning algorithms and navigating in their chemical space, Scientific Reports 11(1) (2021) 7628.
[39] S. Guha, K. Majumder, Structural-features of food-derived bioactive peptides with anti-inflammatory activity: A brief review, Journal of Food Biochemistry 43(1) (2019) e12531.
[40] H.J. Vogel, D.J. Schibli, W. Jing, E.M. Lohmeier-Vogel, R.F. Epand, R.M. Epand, Towards a structure-function analysis of bovine lactoferricin and related tryptophan- and arginine-containing peptides, Biochemistry and Cell Biology 80(1) (2002) 49-63.
[41] L. Zhao, X. Wang, X.-L. Zhang, Q.-F. Xie, Purification and identification of anti-inflammatory peptides derived from simulated gastrointestinal digests of velvet antler protein (Cervus elaphus Linnaeus), Journal of Food and Drug Analysis 24(2) (2016) 376-384.
[42] K. Majumder, S. Chakrabarti, S.T. Davidge, J. Wu, Structure and Activity Study of Egg Protein Ovotransferrin Derived Peptides (IRW and IQW) on Endothelial Inflammatory Response and Oxidative Stress, Journal of Agricultural and Food Chemistry 61(9) (2013) 2120-2129.
[43] Q.Z. Huanli Jiao, Yuanbang Lin, Ying Gao, Peng Zhang, , The Ovotransferrin-Derived Peptide IRW Attenuates Lipopolysaccharide-Induced Inflammatory Responses, Biomed Res Int (2019).
[44] S. Chen, S. Bonifati, Z. Qin, C. St. Gelais, K.M. Kodigepalli, B.S. Barrett, S.H. Kim, J.M. Antonucci, K.J. Ladner, O. Buzovetsky, K.M. Knecht, Y. Xiong, J.S. Yount, D.C. Guttridge, M.L. Santiago, L. Wu, SAMHD1 suppresses innate immune responses to viral infections and inflammatory stimuli by inhibiting the NF-κB and interferon pathways, Proceedings of the National Academy of Sciences 115(16) (2018) E3798-E3807.
[45] K. Aihara, H. Ishii, M. Yoshida, Casein-derived tripeptide, Val-Pro-Pro (VPP), modulates monocyte adhesion to vascular endothelium, Journal of Atherosclerosis and Thrombosis 16(5) (2009) 594-603.
[46] H.J. Chung, J. Lee, J.S. Shin, M.R. Kim, W. Koh, M.J. Kim, J.W. Lee, E.J. Kim, I.H. Lee, W.K. Kim, Y.J. Lee, S.K. Lee, I.H. Ha, In Vitro and In Vivo Anti-Allergic and Anti-Inflammatory Effects of eBV, a Newly Developed Derivative of Bee Venom, through Modulation of IRF3 Signaling Pathway in a Carrageenan-Induced Edema Model, PLoS One 11(12) (2016) e0168120.
[47] L. Fu, L. Xing, Y. Hao, Z. Yang, S. Teng, L. Wei, W. Zhang, The anti-inflammatory effects of dry-cured ham derived peptides in RAW264.7 macrophage cells, Journal of Functional Foods 87 (2021) 104827.

[48] J. Han, R.J. Ulevitch, Emerging targets for anti-inflammatory therapy, Nature Cell Biology 1(2) (1999) E39-E40.
[49] N. Kumar, S. Reddi, S. Devi, S.B. Mada, R. Kapila, S. Kapila, Nrf2 dependent antiaging effect of milk-derived bioactive peptide in old fibroblasts, Journal of Cellular Biochemistry 120(6) (2019) 9677-9691.
[50] K.D. Saint Jean, K.D. Henderson, C.L. Chrom, L.E. Abiuso, L.M. Renn, G.A. Caputo, Effects of Hydrophobic Amino Acid Substitutions on Antimicrobial Peptide Behavior, Probiotics Antimicrob Proteins 10(3) (2018) 408-419.
[51] M. Mahlapuu, J. Håkansson, L. Ringstad, C. Björn, Antimicrobial Peptides: An Emerging Category of Therapeutic Agents, Frontiers in Cellular and Infection Microbiology 6(194) (2016).
[52] D. Mohanty, R. Jena, P.K. Choudhury, R. Pattnaik, S. Mohapatra, M.R. Saini, Milk Derived Antimicrobial Bioactive Peptides: A Review, International Journal of Food Properties 19(4) (2016) 837-846.
[53] T. Ahmed, R. Hammami, Recent insights into structure–function relationships of antimicrobial peptides, Journal of Food Biochemistry 43(1) (2019) e12546.
[54] P.A.B. Branco, Purification and biochemical/molecular characterisation of antimicrobial peptides produced by Saccharomyces cerevisiae and evaluation of their mode of action, Lisboa:ISA (2018) 246 P.
[55] Q.-Y. Zhang, Z.-B. Yan, Y.-M. Meng, X.-Y. Hong, G. Shao, J.-J. Ma, X.-R. Cheng, J. Liu, J. Kang, C.-Y. Fu, Antimicrobial peptides: mechanism of action, activity and clinical potential, Military Medical Research 8(1) (2021) 48.
[56] C. Imjongjirak, P. Amphaiphan, W. Charoensapsri, P. Amparyup, Characterization and antimicrobial evaluation of SpPR-AMP1, a proline-rich antimicrobial peptide from the mud crab Scylla paramamosain, Developmental & Comparative Immunology 74 (2017) 209-216.
[57] I. Unalan, B. Slavik, A. Buettner, W.H. Goldmann, G. Frank, A.R. Boccaccini, Physical and Antibacterial Properties of Peppermint Essential Oil Loaded Poly (ε-caprolactone) (PCL) Electrospun Fiber Mats for Wound Healing, Frontiers in Bioengineering and Biotechnology 7 (2019).
[58] J. Martin, A. Desfoux, J. Martinez, M. Amblard, A. Mehdi, L. Vezenkov, G. Subra, Bottom-up strategies for the synthesis of peptide-based polymers, Progress in Polymer Science 115 (2021) 101377.
[59] N.E. Zander, J.A. Orlicki, A.M. Rawlett, T.P. Beebe, Jr., Surface-modified nanofibrous biomaterial bridge for the enhancement and control of neurite outgrowth, Biointerphases 5(4) (2010) 149-58.
[60] K. Sivaraman, K. Muthukumar, C. Shanthi, A potential bioactive peptide candidate for biomaterial and tissue engineering applications, Life Sciences 226 (2019) 140-148.
[61] S.G. Kumbar, S.P. Nukavarapu, R. James, L.S. Nair, C.T. Laurencin, Electrospun poly(lactic acid-co-glycolic acid) scaffolds for skin tissue engineering, Biomaterials 29(30) (2008) 4100-4107.
[62] R. Bucci, F. Vaghi, E. Erba, A. Romanelli, M.L. Gelmi, F. Clerici, Peptide grafting strategies before and after electrospinning of nanofibers, Acta Biomaterialia 122 (2021) 82-100.
[63] J. Lee, H. Byun, S.K. Madhurakkat Perikamana, S. Lee, H. Shin, Current Advances in Immunomodulatory Biomaterials for Bone Regeneration, Adv Healthc Mater 8(4) (2019) e1801106.
[64] D.G.N. Ghobeira R, Morent R. , Plasma surface functionalization of biodegradable electrospun scaffolds for tissue engineering applications, IAPC Publishing, Croatia, 2017.

[65] H.-S. Lee, S.J. Stachelek, N. Tomczyk, M.J. Finley, R.J. Composto, D.M. Eckmann, Correlating macrophage morphology and cytokine production resulting from biomaterial contact, Journal of biomedical materials research. Part A 101(1) (2013) 203-212.
[66] G. Zhou, T. Groth, Host Responses to Biomaterials and Anti-Inflammatory Design-a Brief Review, Macromol Biosci 18(8) (2018) e1800112.
[67] F.Y. McWhorter, T. Wang, P. Nguyen, T. Chung, W.F. Liu, Modulation of macrophage phenotype by cell shape, Proceedings of the National Academy of Sciences of the United States of America 110(43) (2013) 17253-17258.
[68] J.S. Stevens, A.C. de Luca, S. Downes, G. Terenghi, S.L.M. Schroeder, Immobilisation of cell-binding peptides on poly-ε-caprolactone (PCL) films: A comparative XPS study of two chemical surface functionalisation methods, Surface and Interface Analysis 46(10-11) (2014) 673-678.
[69] K.M. Hotchkiss, G.B. Reddy, S.L. Hyzy, Z. Schwartz, B.D. Boyan, R. Olivares-Navarrete, Titanium surface characteristics, including topography and wettability, alter macrophage activation, Acta Biomater 31 (2016) 425-434.
[70] F.Y. McWhorter, T. Wang, P. Nguyen, T. Chung, W.F. Liu, Modulation of macrophage phenotype by cell shape, Proc Natl Acad Sci U S A 110(43) (2013) 17253-8.
[71] P. Everts, K. Onishi, P. Jayaram, J.F. Lana, K. Mautner, Platelet-Rich Plasma: New Performance Understandings and Therapeutic Considerations in 2020, Int J Mol Sci 21(20) (2020) 7794.

Fig. 1- Viability of macrophages (A) and fibroblasts (B) in the presence of different concentrations (0.25, 0.5, and 1mM) of peptides at different periods. Comparison between the proliferative effect of peptides at the concentration of 0.25 mM after 24 h on U937 (C-I) and comparison between the highest proliferation effect of the peptides on fibroblasts (C-II) after 24 h. Cell viability was measured using Cell Titer Glo Luminescent cell viability assay kit. The percent of proliferation in all samples is calculated in comparison with the control sample. Results are presented as mean±SEM obtained from three biological replications. Different letters present the significant differences between data at $P<0.05$.

Fig.2- Effects of peptides at a final concentration of 0.5 mM on LPS-induced level of TNF-α in macrophages as measured by intracellular flow cytometry assay (A and B-I). Effect of peptides on level of IFN-γ stimulated level of CD64 as measured by flow cytometry method and expressed as median fluorescence intensity (MFI) (B-II). LPS-induced level of TNF-α (B-III) and IL-6 (B-IV) as measured by ELISA. Flow cytometry data are obtained from three biological replications. ELISA data are obtained from two biological and three ELISA assay replications. Results are presented as mean±SEM. * $P<0.05$, **$P<0.01$, *** $P<0.005$, and ****$P<0.001$ present the significant differences between data and control sample (blue column).

Fig. 3. Effect of the peptides (0.5 mM) on Collagen synthesis by human skin fibroblasts measured by the Collagen assay kit (A). Scratch wound assay using human skin fibroblast cell lines incubated with peptides (0.5 mM) for 24 h. The pictures were taken using a Zeiss AxioObserver Z1 (inverted wide-field microscope), with a 10x/0.3 EC Plan Neofluar Dry Ph1 objective during 24 h. The covered areas were measured with the WimScratch software program (Wimasis, Munich, Germany), and the percent increase in cell covered area was determined for each sample after 16 and 24 h compared to time zero **(B and C)**. Results are presented as mean±SEM obtained from three biological replications. Different letters present the significant differences between data ($P<0.05$).

Fig. 4. Functionalization of PCL scaffold with VW-9 through CDI (A) and Thiol (B) chemistry. FTIR of unmodified PCL (A0), peptide functionalized PCL by carbodiimide reaction (A1), peptide functionalized PCL by thiol reaction (A4), and peptide functionalized PCL by physical method (A7). Red boxes highlight the IR transmittance peaks at 3200 cm^{-1} and 1630 cm^{-1} that indicates the amide bonds associated with the peptide (C). Peptide release from A7 scaffolds measured by MS-spectrophotometric method (D). MS-Spectrophotometric analysis of scaffolds after heat treatment at printing conditions (E). SEM images of scaffolds microstructure before and after plasma treatment (F). XPS analysis of Carbon and Oxygen elements before and after plasma treatment (G).

Fig. 5. Scaffold microstructure as seen with a scanning electron microscope (SEM). Images were taken to see how the surface of the scaffolds looked and to see if there were any morphological variations. Each sample is replicated three times.

Fig. 6. Representative fluorescence microscopy images of PCL scaffolds containing peptides conjugated with biotin and labeled with streptavidin-FITC (green), as well as the quantification of mean fluorescence intensity in different scaffolds. Each sample is replicated three times.

Fig. 7. Cell viability of macrophage (A) and fibroblast (B) on peptide-functionalized PCL prepared by CDI chemistry (I), thiol chemistry (II), and physical (III) methods in comparison with native PCL (A0**)** as control. The CellTiter 96 AQueous one solution proliferation assay (MTS) kit is used for determination of cell viability. Results are presented as mean±SEM. * $P<0.05$, **$P<0.01$, *** $P<0.005$, and ****$P<0.001$ present the significant differences between data.

Fig. 8. Wide-field fluorescence microscopy image of fibroblasts and macrophages on functionalized PCL (A2 and A3) in comparison to native PCL (A0). Rhodamine-phalloidin and DAPI were used to mark fiber scaffolds seeded with macrophages and fibroblasts. Actin filaments and nuclei were stained separately.

Fig. 9. SEM images of macrophages cultured for 48 h on native PCL (A0) and peptide functionalized PCL (A1, A3, A4, A5, A7) fibers (scale bar=100, 50, and 10 µm) .

Fig. 10. SEM images of macrophages cultured for 48 h on native PCL (A0) and peptide functionalized PCL (A2 and A3) fibers (scale bar=20 and 10 µm).

Fig. 11. The level of IL-6 **(A)** and TNF-α **(B)** in non-treated and LPS treated free cells as well as in LPS-stimulated cells cultured on natural (A0) and peptide-functionalized PCL. Data are obtained from three biological and three ELISA assay replications. Results are presented as mean±SEM. * $P<0.05$, ** $P<0.01$, *** $P<0.005$, and **** $P<0.001$ present the significant differences between natural PCL as control (A0) and peptide-functionalized PCL. `

Fig. 12. The images of *in vivo* wound closure studies for negative control (C-), PRP (C+) and peptide (VW-9) (P) solutions (**A**), Photomicrographs of histological sections stained with hematoxylin and eosin (H&E) on day 3 and 7 of PRP and peptide groups (5 rats per groups) (**B**), the wound-healing ratio at days 3, 5, and 7 for wound treated with PRP (C+) and peptide (P) in comparison to negative control (C-) (**C**). The images of *in vivo* wound closure studies for negative control (C-), Sorbalgon(C+) and peptide functionalized PCL (T) (**D**), Photomicrographs of histological sections stained with hematoxylin and eosin (H&E) on day 4, 8, 12 and 16 of Sorbalgon and peptide-functionalized PCL groups (5 rats per groups) (**E**), the wound-healing ratio at days 4, 8, 12 and 16 for wound treated with Sorbalgon (C^+) and peptide functionalized PCL (T) in comparison to negative control (C-)(**F**). Data are mean ± standard deviation of five independent experiments.

Figure(s)

Click here to access/download;Figure(s);Figure1A.jpg

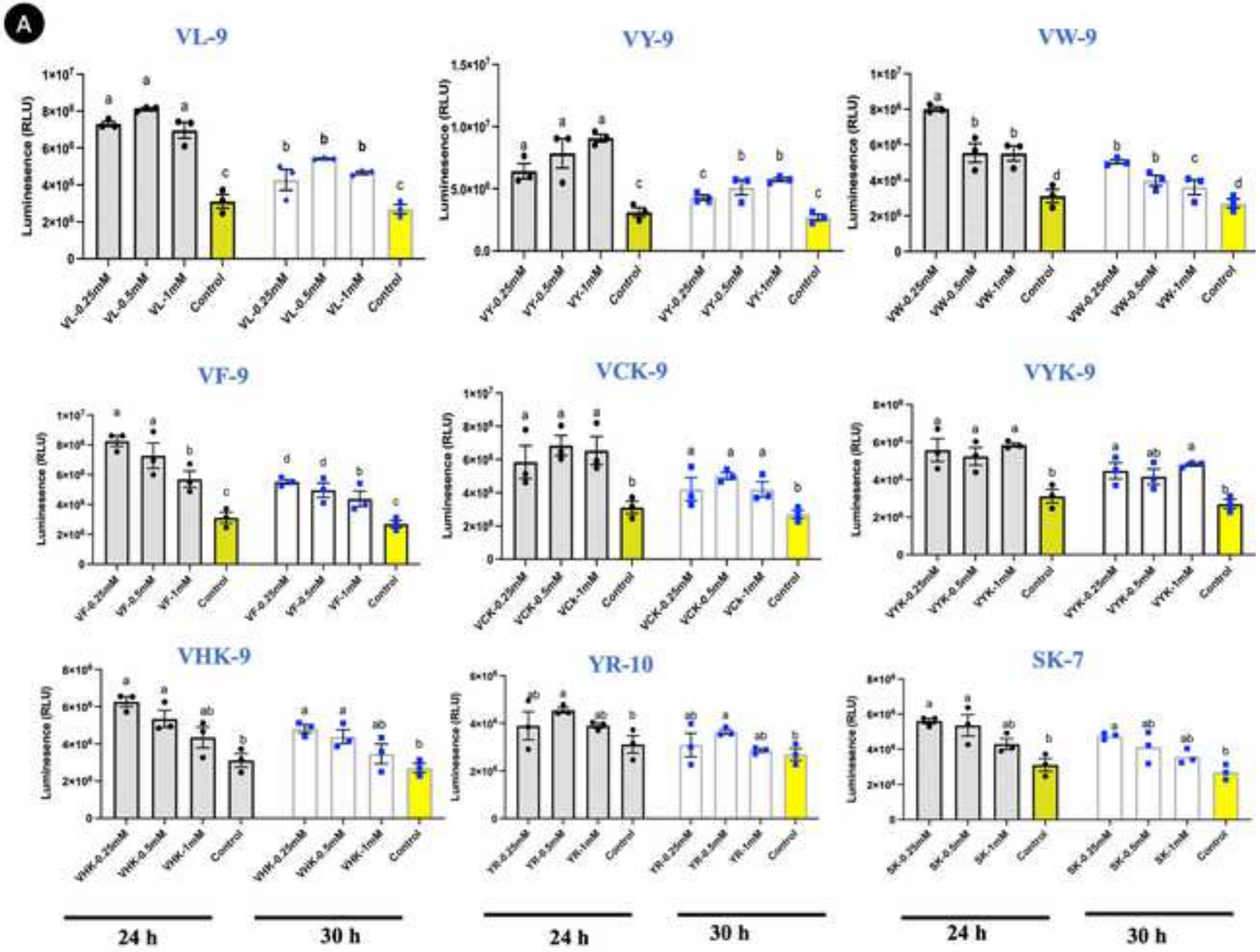

Figure(s)

Click here to access/download;Figure(s);Figure1B.jpg

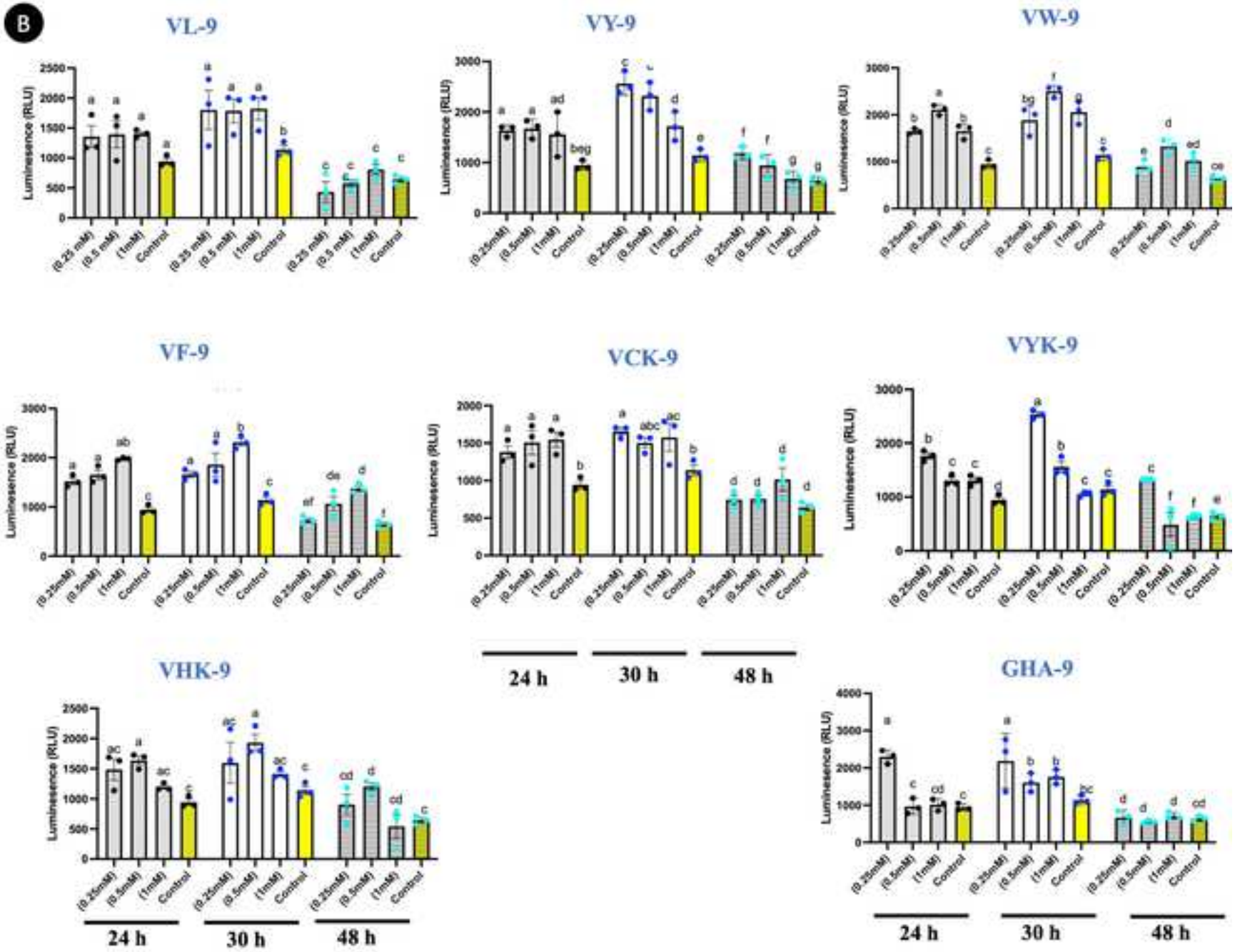

Figure(s)

Click here to access/download;Figure(s);Figure1C.jpg

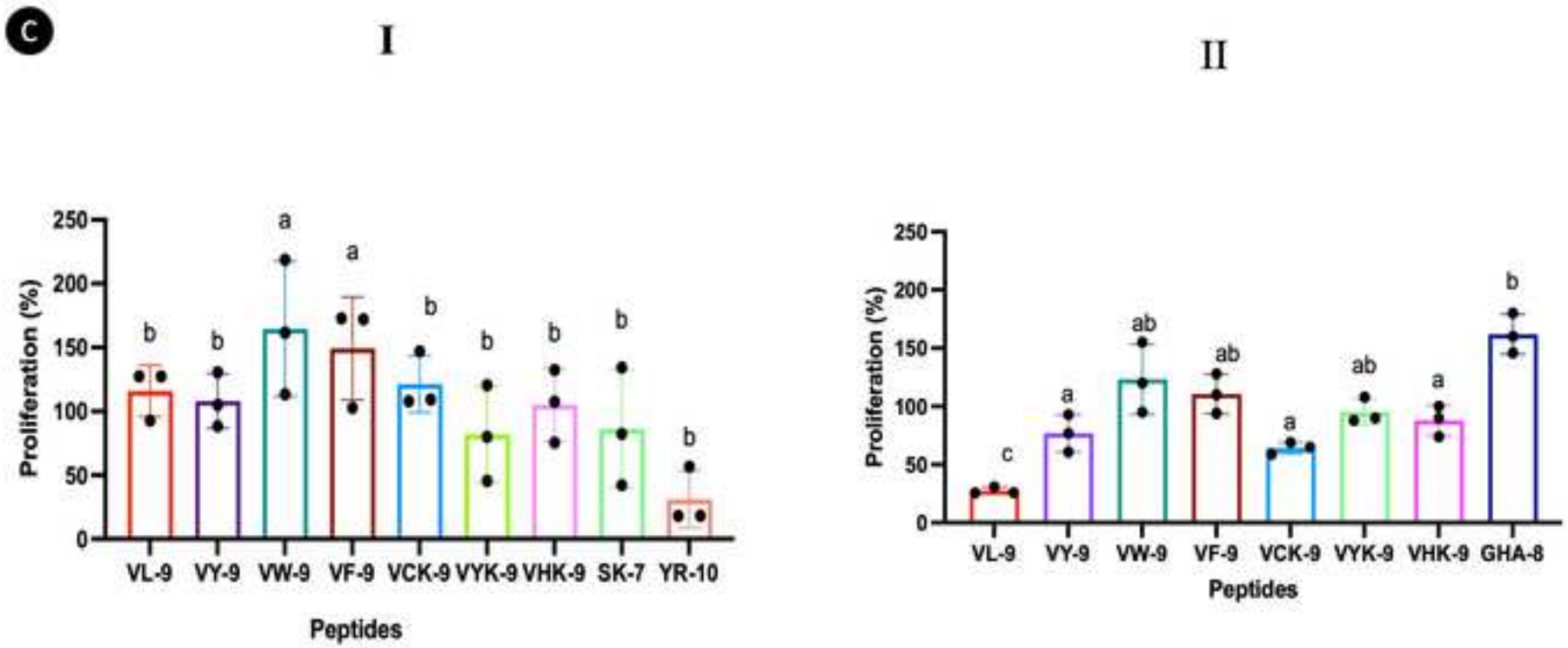

Figure(s)

Click here to access/download;Figure(s);Figure 2A.jpg

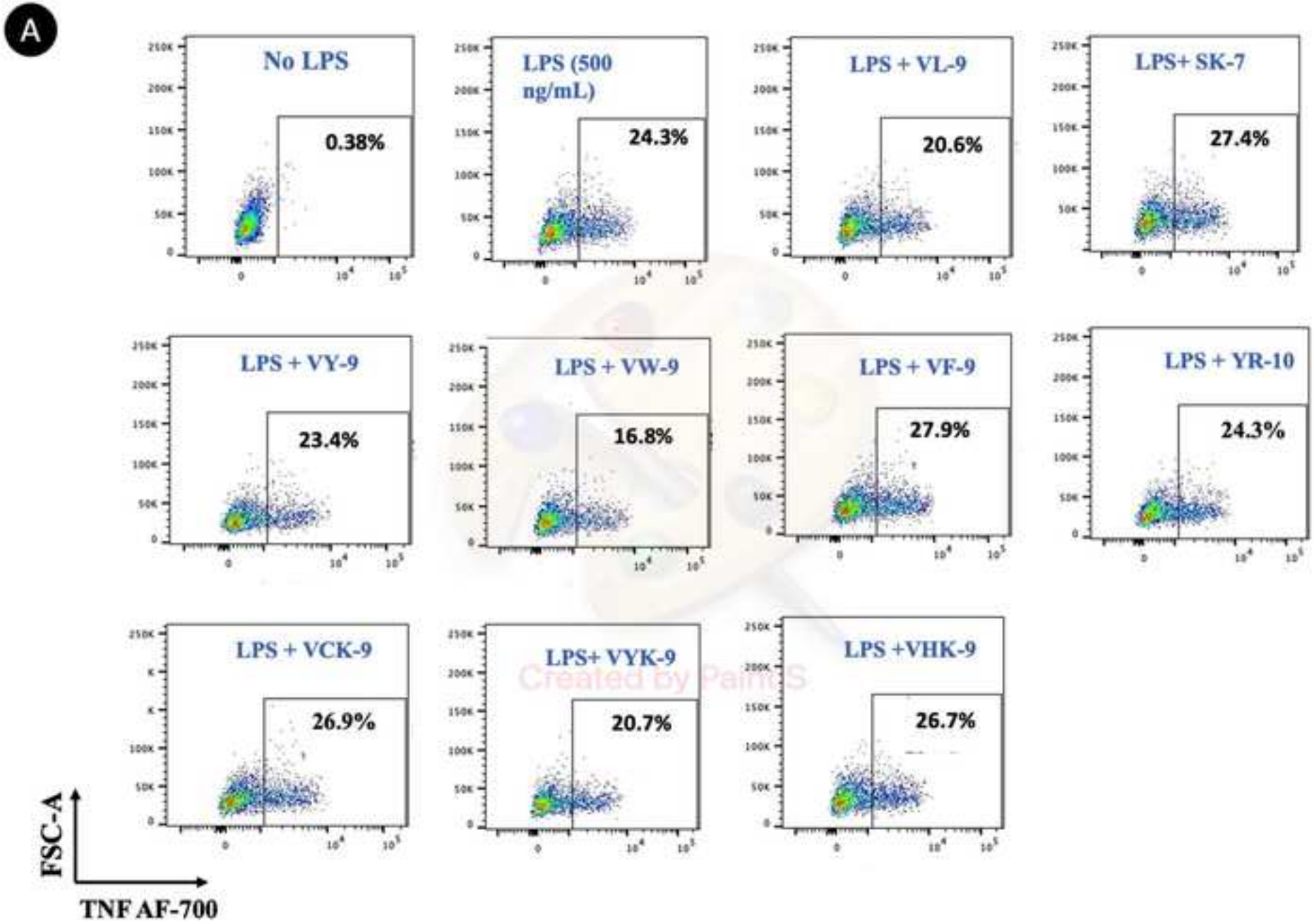

Figure(s)

Click here to access/download;Figure(s);Figure2b.jpg

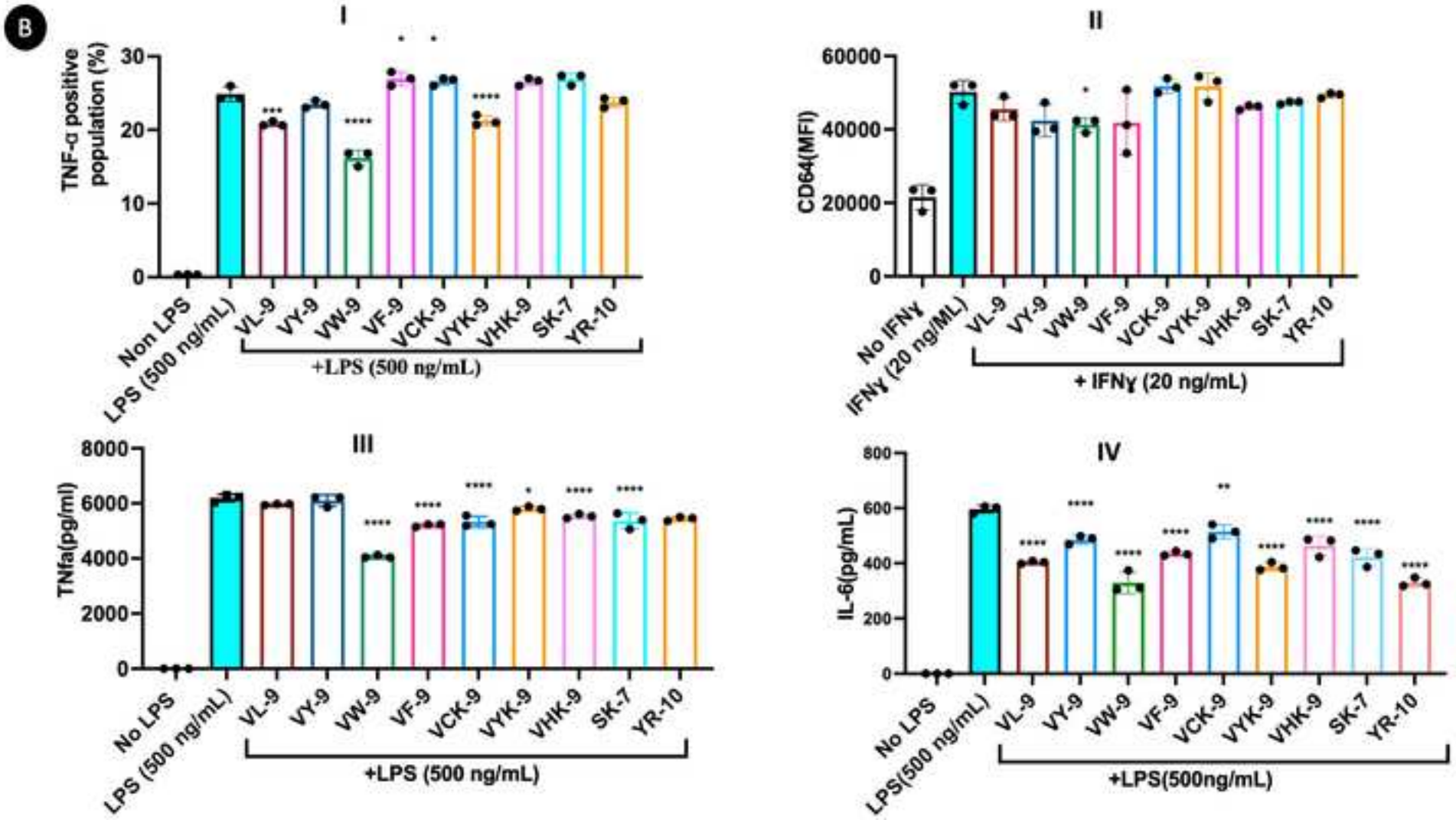

Figure(s)

Click here to access/download;Figure(s);Figure3.jpg

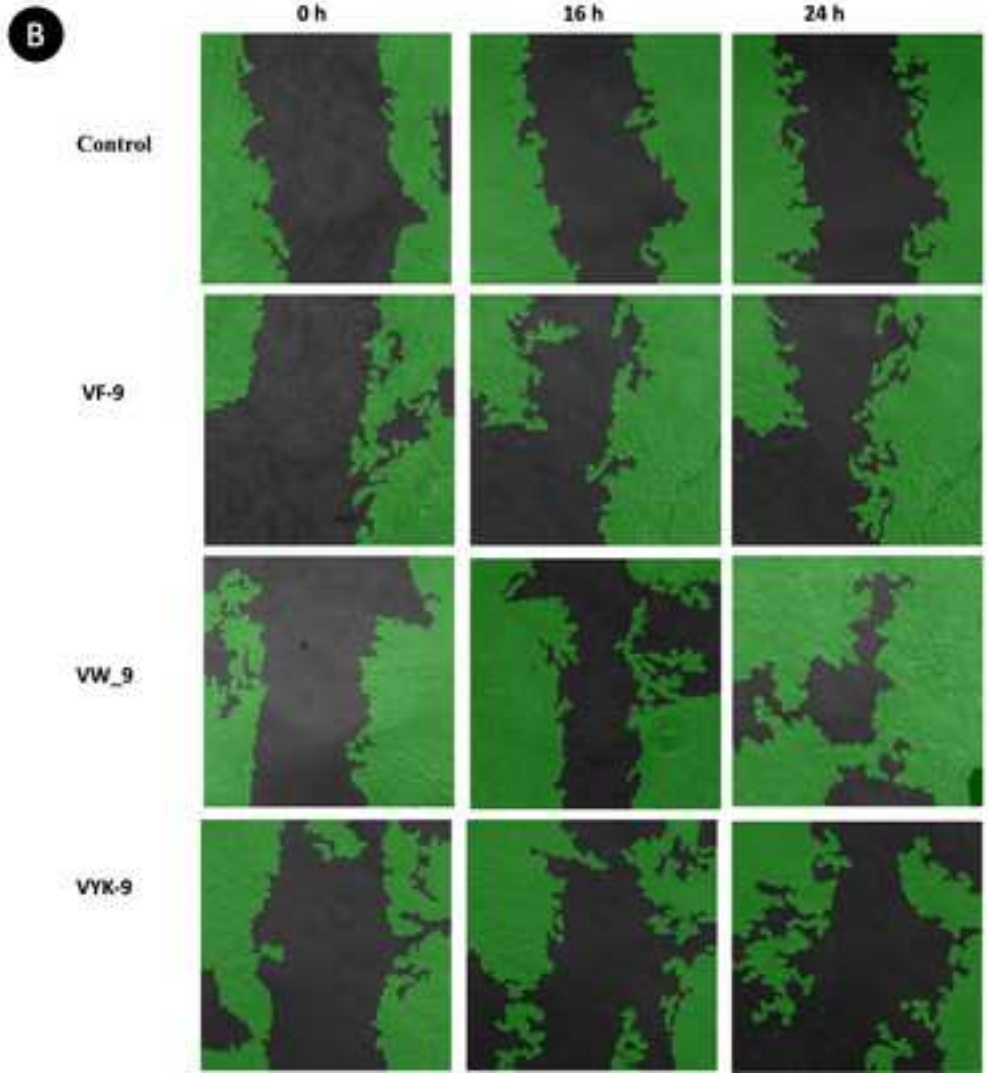

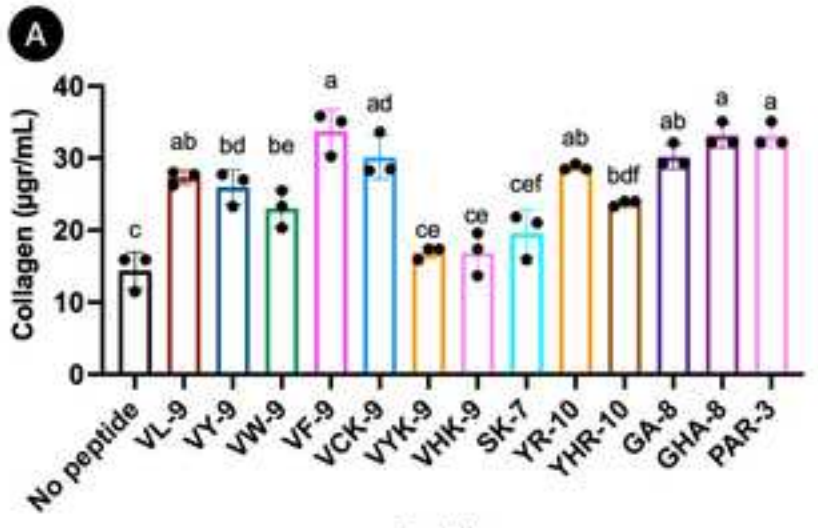

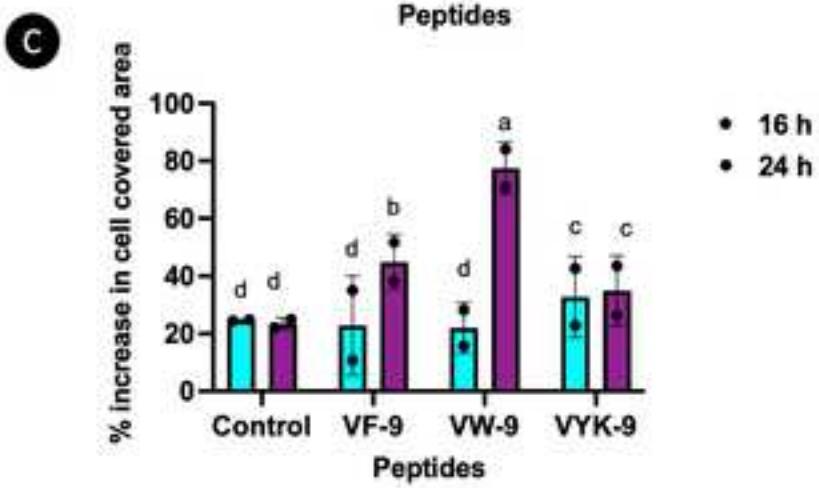

Figure(s)

Click here to access/download;Figure(s);Figure4.jpg

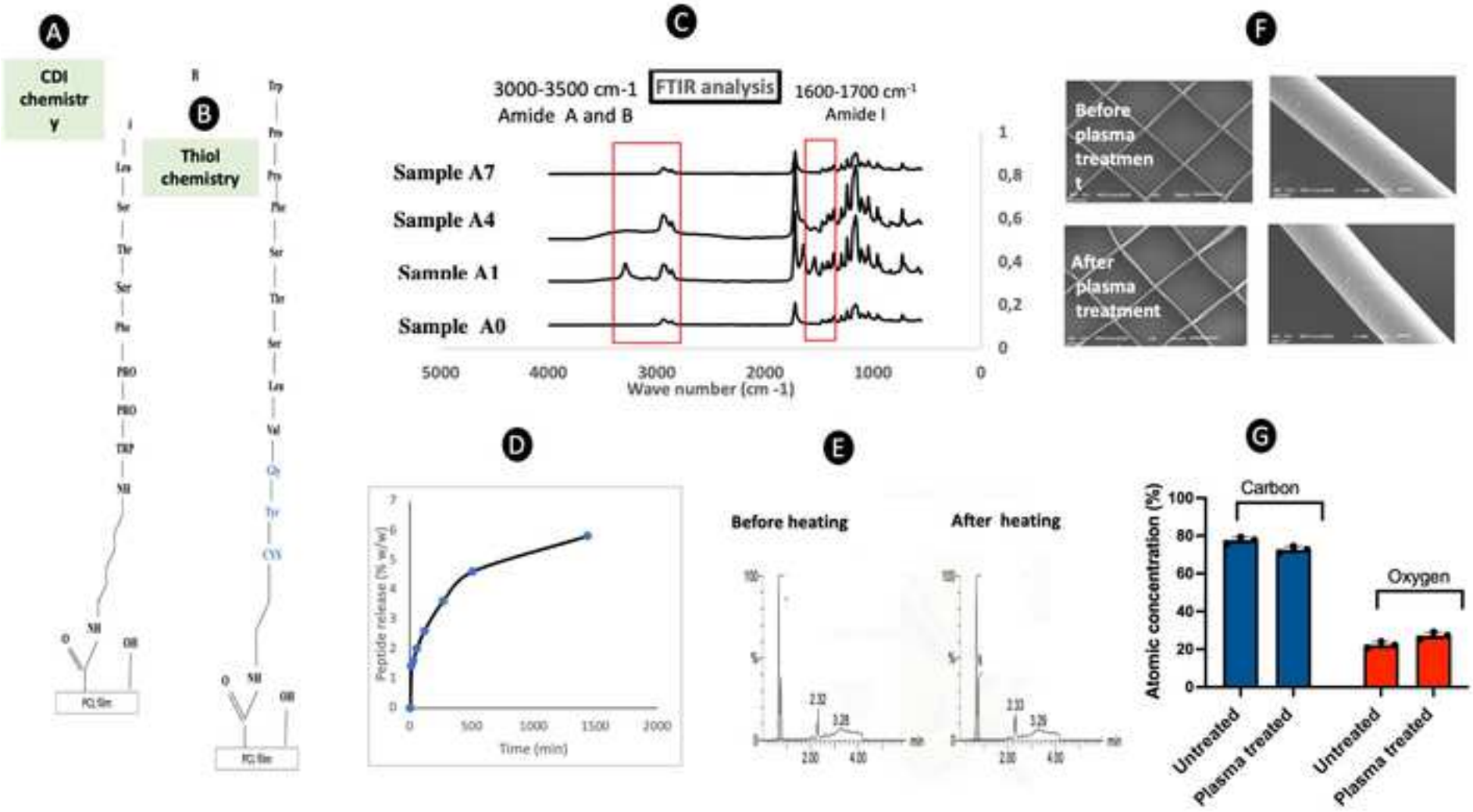

Figure(s)

Click here to access/download;Figure(s);Figure 5.jpg

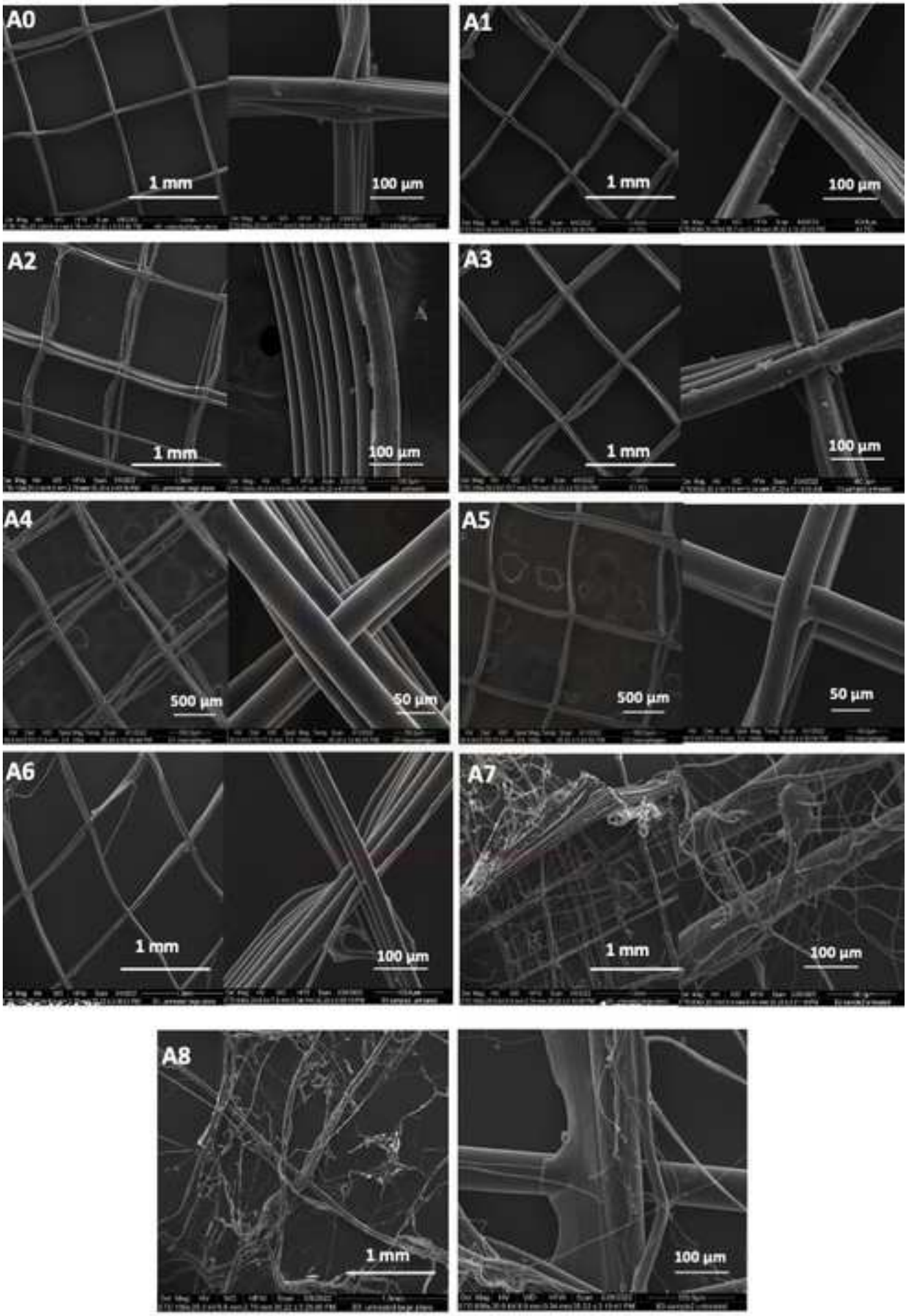

Figure(s)

Click here to access/download;Figure(s);Figure6.jpg

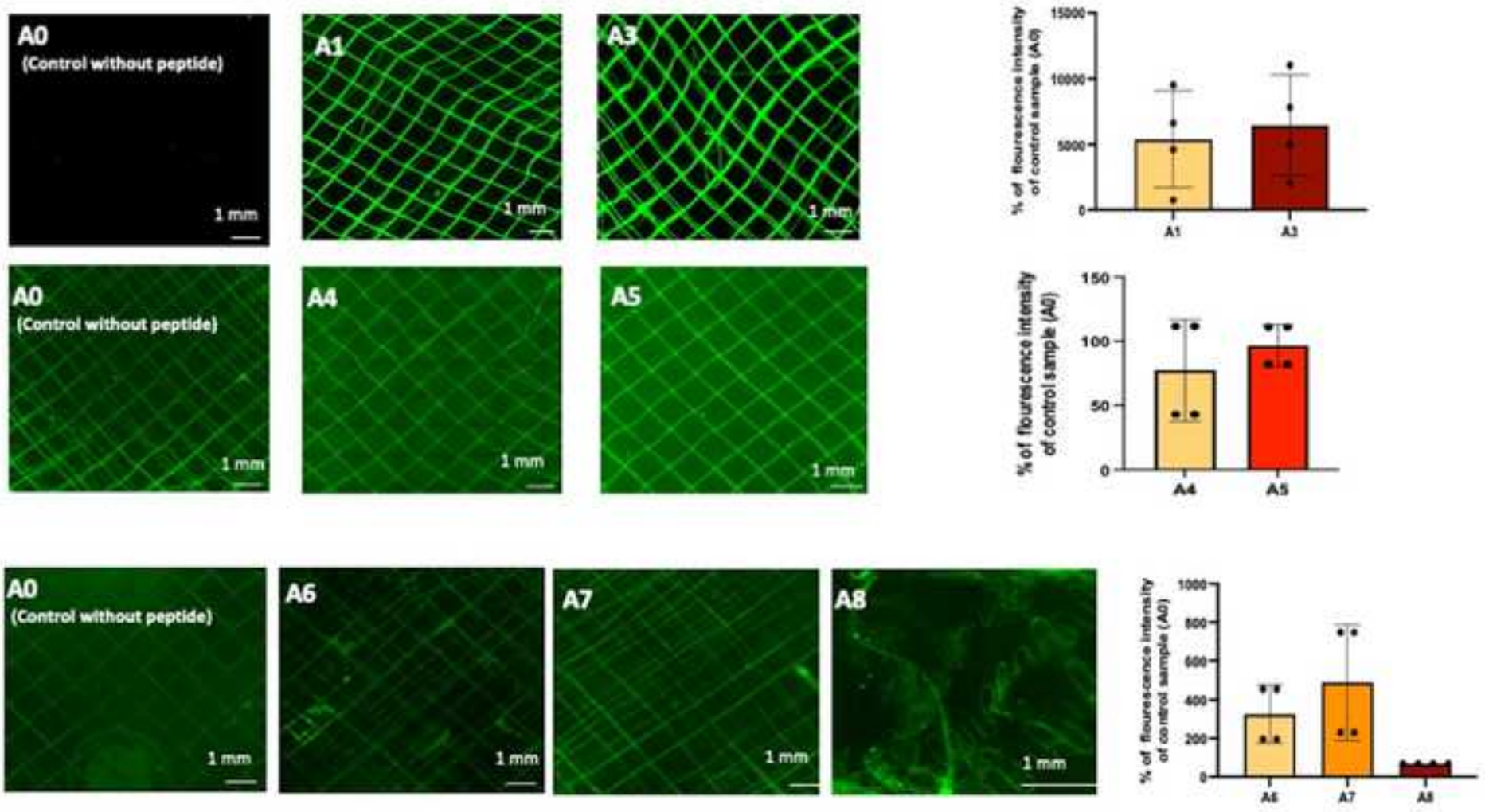

Figure(s)

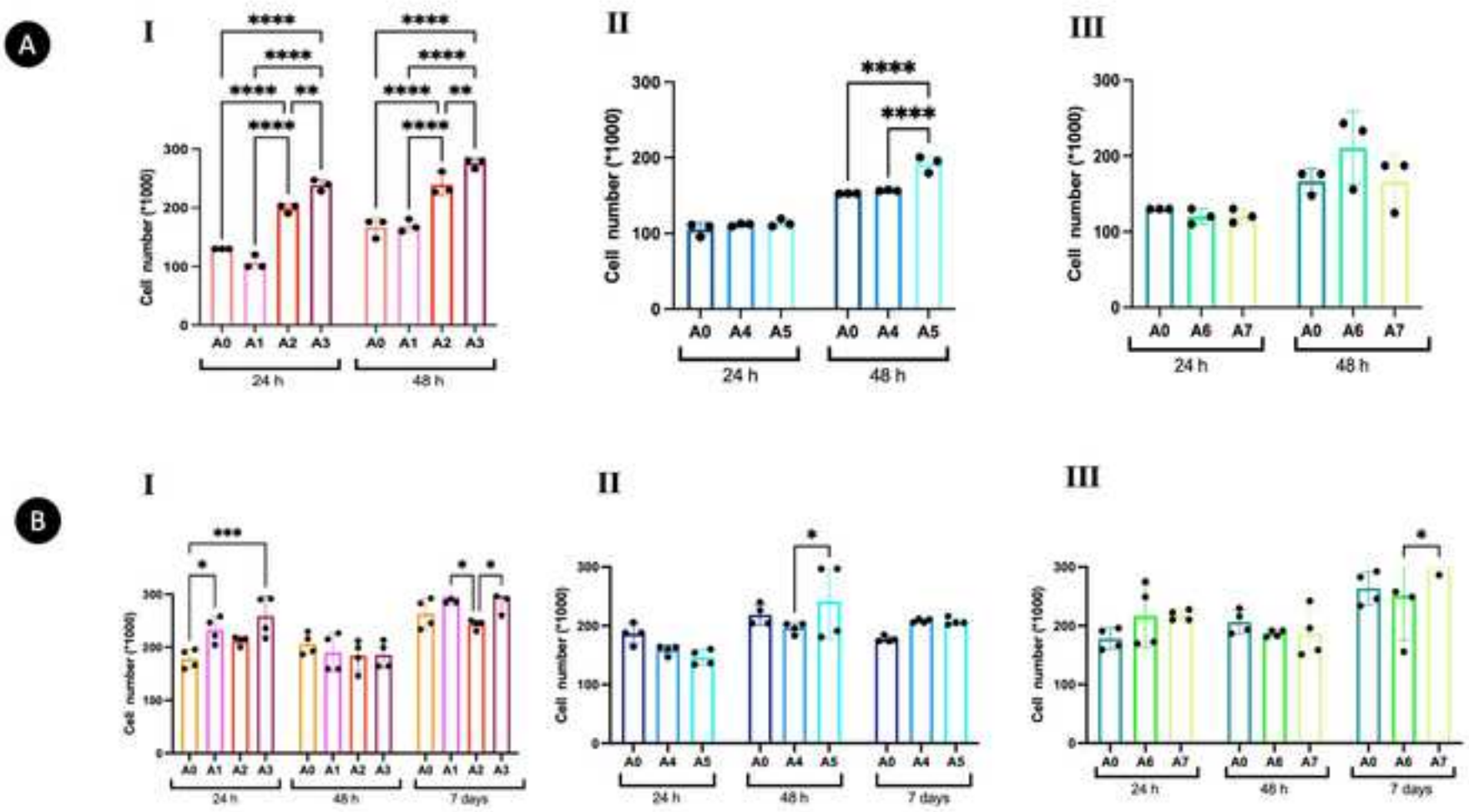

Figure(s)

Click here to access/download;Figure(s);Figure8.jpg

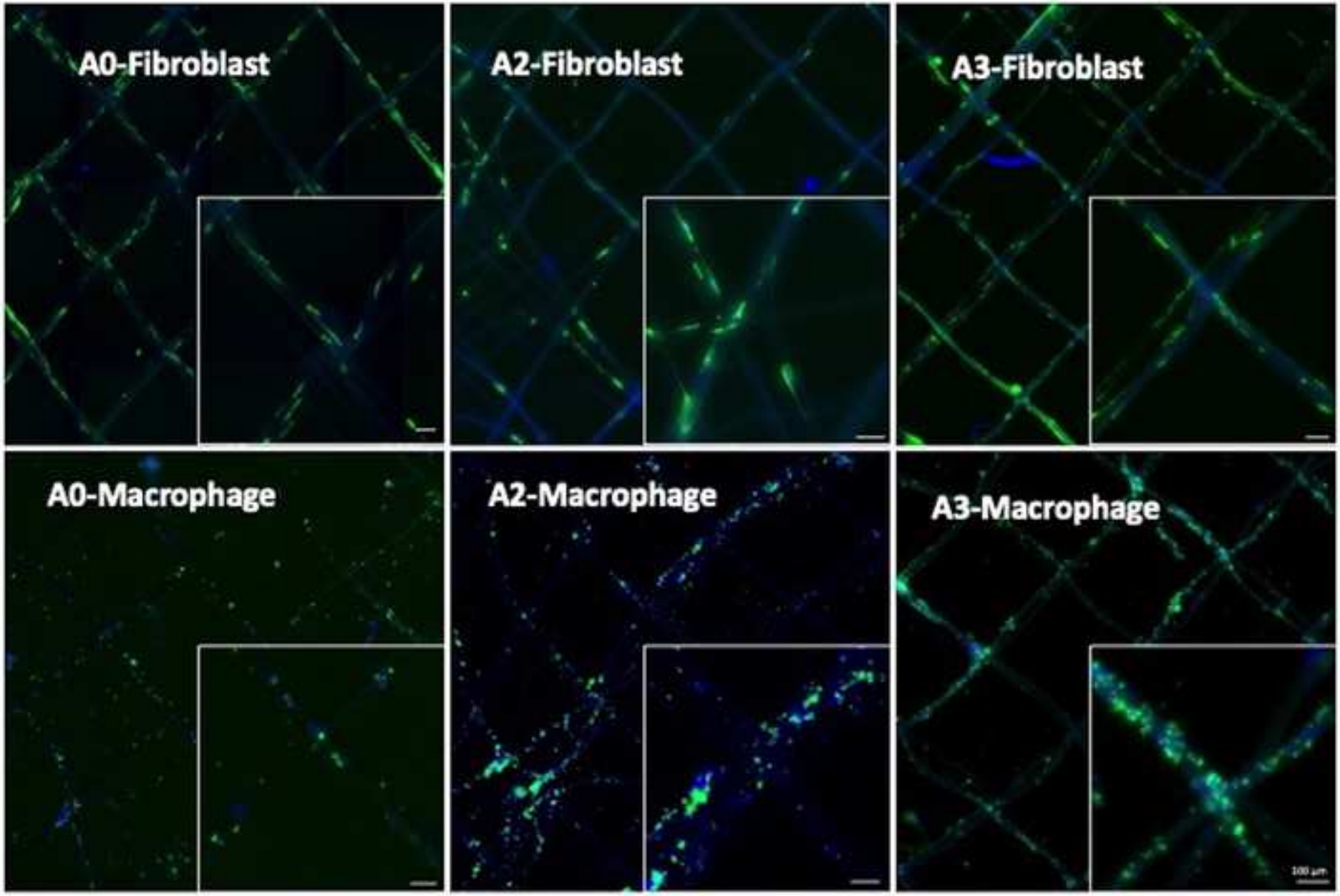

Figure(s)

Click here to access/download;Figure(s);Figure9.jpg

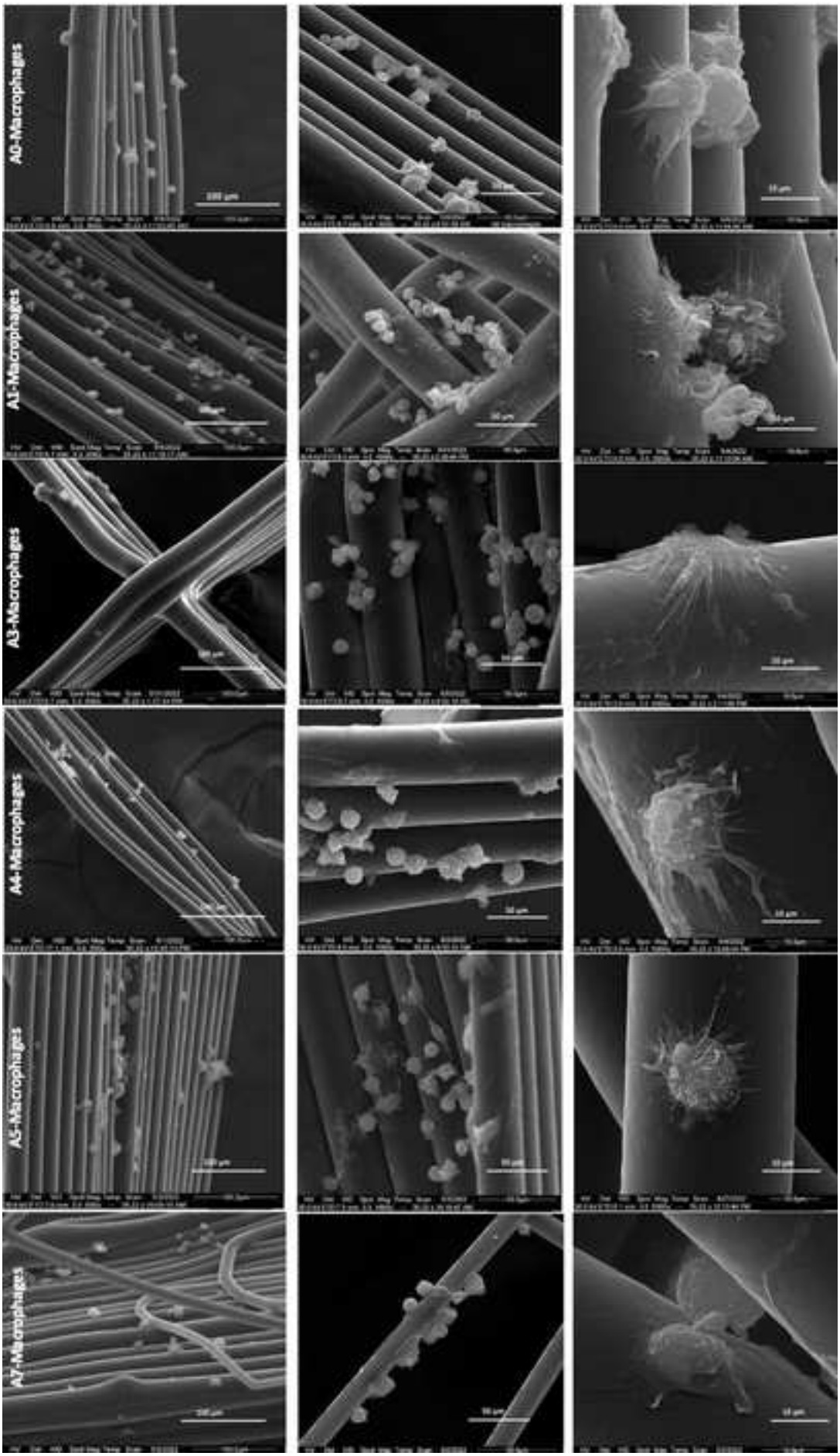

Figure(s)

Click here to access/download;Figure(s);Figure10.jpg

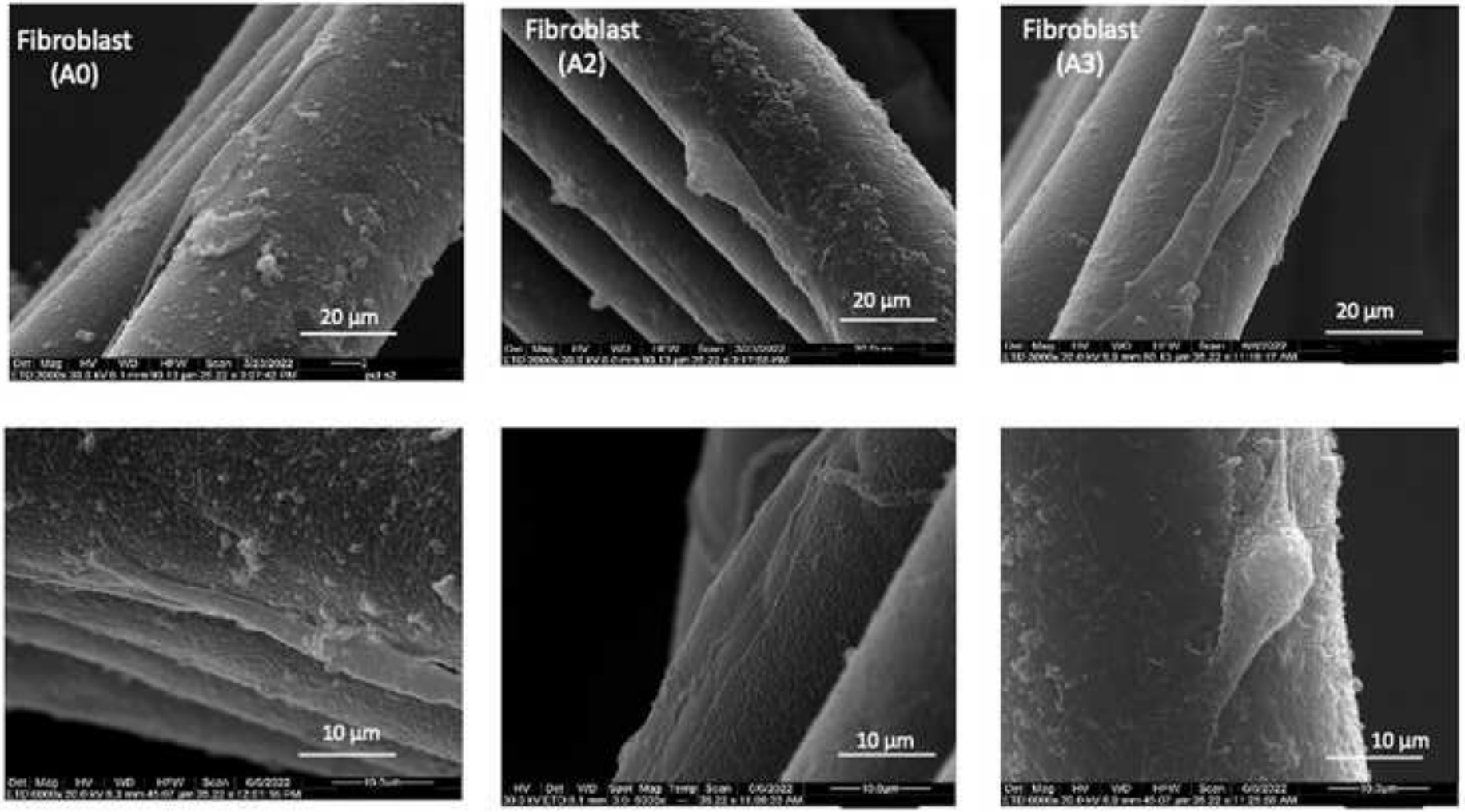

Figure(s)

Click here to access/download;Figure(s);Figure11.jpg